ACCURATE BUCKLING ANALYSIS OF PIEZOELECTRIC FUNCTIONALLY
GRADED NANOTUBE-REINFORCED CYLINDRICAL SHELLS UNDER
COMBINED ELECTRO-THERMO-MECHANICAL LOADS

Shengbo Zhu, Yiwen Ni, Jiabin Sun, Zhenzhen Tong, Zhenhuan Zhou and Xinsheng Xu

ACCURATE BUCKLING ANALYSIS OF PIEZOELECTRIC FUNCTIONALLY GRADED NANOTUBE-REINFORCED CYLINDRICAL SHELLS UNDER COMBINED ELECTRO-THERMO-MECHANICAL LOADS

SHENGBO ZHU, YIWEN NI, JIABIN SUN,
ZHENZHEN TONG, ZHENHUAN ZHOU AND XINSHENG XU

An accurate axial buckling analysis of piezoelectric functionally graded nanotube-reinforced composite cylindrical shells under combined electro-thermo-mechanical loads is performed in the Hamiltonian system. The Hamiltonian form of governing buckling equations is established based on the symplectic geometry and Reissner's shell theory. Exact solutions are expressed in terms of symplectic eigenfunctions which have five possible forms. A detailed parametric study is conducted to demonstrate the influences of geometrical parameters, boundary conditions, reinforcement nanotubes and their distribution patterns on the symplectic eigenfunctions. Furthermore, the effects of distribution patterns of nanotubes, electric voltage and temperature rise on critical buckling stresses are investigated.

1. Introduction

In recent years, nanocomposite have received increasingly attention in both scientific and industrial communities [Zeighampour and Tadi Beni 2014; Tadi Beni et al. 2015; 2016; Tadi Beni and Mehralian 2016; Mehralian et al. 2016a; 2016b; 2017a; 2017b; Mehralian and Tadi Beni 2016; 2017a; 2017b; 2018; Jamal-Omidi and ShayanMehr 2017; Kheibari and Beni 2017; Hajmohammad et al. 2018; Kamarian et al. 2018; Rafiee et al. 2019]. Piezoelectric polymers, as a kind of piezoelectric composite, usually offer low density, high toughness and high electromechanical effects, which cannot be realized with piezoelectric ceramics or single crystals [Ueberschlag 2001]. Recently, in order to enhance the performance of such piezoelectric polymers, boron nitride nanotubes (BNNTs) and carbon nanotubes (CNTs) with functionally graded (FG) distribution in the matrix were introduced to reinforce the piezoelectric polymer [Ghorbanpour Arani et al. 2016; Mohammadimehr et al. 2016]. The strength, electrical and thermal conductivity of piezoelectric FG nanotube reinforced composites (NTRC) are greatly improved so that the proposed composites become potential candidates for fabricating the key component of intelligent devices and equipment, such as FG-NTRC hybrid laminated beams [Fan and Wang 2016], FG-NTRC beams with piezoelectric layers [Rafiee et al. 2013; Yang et al. 2015; Wu et al. 2016] and FG-NTRC plates with piezoelectric layers [Rafiee et al. 2014; Wu and Chang 2014; Mohammadimehr et al. 2016; Hajmohammad et al. 2017; Keleshteri et al. 2017]. The cylindrical shells made of piezoelectric FG-NTRC are also ones of the important fundamental components. Hence, the stability analysis of piezoelectric FG-NTRC cylindrical shells under combined electro-thermo-mechanical loads is of great importance for the design and evaluation of the fundamental structures.

The nature for buckling of piezoelectric cylindrical shells has been well studied in the literature. Mohammadimehr et al. [2014], Ganesan and Kadoli [2003], Sheng and Wang [2010] investigated the buckling of piezoelectric FG cylindrical shells by using the finite element method. Mirzavand et al. [2016], Fard and Bohlooly [2017], Sun et al. [2016; 2018] investigated the axial buckling, thermal buckling and postbuckling of piezoelectric cylindrical shells by the Galerkin method. Dai and Zheng [2011] analyzed the buckling and postbuckling of piezoelectric fiber reinforced composite cylindrical shell by the Ritz energy method. Mehralian et al. [2016a] investigated the buckling of anisotropic piezoelectric cylindrical shells by using the generalized differential quadrature (GDQ) method. Farajpour et al. [2017] investigated the vibration, buckling and smart control of piezoelectric nanoshells by using the GDQ method. Zhu et al. [2017] investigated the size-dependent effect on the torsional buckling of FG cylindrical nanoshell covered with piezoelectric nanolayers by using the GDQ method. Mirzavand et al. [2010; 2013], Dai et al. [2013] investigated the thermal buckling and postbuckling of piezoelectric FG cylindrical shells by using the finite difference method. Shen [2001; 2002a; 2002b; 2005; 2009; 2010], Shen and Li [2002], Shen and Noda [2007], Shen and Xiang [2007] analyzed the buckling and postbuckling of piezoelectric FG cylindrical shells by the singular perturbation method. Sahmani et al. [2016] studies the nonlinear buckling and postbuckling of piezoelectric cylindrical nanoshells by using the singular perturbation method. Mirzavand and Eslami [2007; 2011], Khoa et al. [2019] obtained exact solutions for buckling and postbuckling of piezoelectric FG cylindrical shells.

In contrast, there are only a few studies on the stability behaviors of piezoelectric shells made of NTRC. Ghorbanpour Arani et al. [2012a; 2012b; 2014] and MosallaieBarzoki et al. [2012; 2013] investigated the axial buckling, torsional buckling and dynamic buckling of piezoelectric NTRC cylindrical shells under electro-thermo-mechanical loads by using the energy method and harmonic differential quadrature method. Salehi-Khojin and Jalili [2008] obtained exact solutions for buckling of simply supported piezoelectric NTRC cylindrical shells under electro-thermo-mechanical loads. For the piezoelectric FG-NTRC, most of the existing literature were concentrated on the buckling of beams or plates [Rafiee et al. 2013; 2014; Wu and Chang 2014; Yang et al. 2015; Fan and Wang 2016; Mohammadimehr et al. 2016; Wu et al. 2016; Hajmohammad et al. 2017; Keleshteri et al. 2017]. The stability of piezoelectric FG-NTRC cylindrical shells was rarely reported in the open literature. Ansari et al. [2016] investigated the postbuckling of FG-NTRC cylindrical shells with piezoelectric layers under electro-thermo-mechanical loads by using the Ritz energy approach. Ninh [2018] analyzed the thermal torsional postbuckling of FG-NTRC cylindrical shells with sur-bonding piezoelectric layers by using the Galerkin method. SafarPour et al. [2019] obtained critical external voltage of rotating piezoelectric FG-NTRC cylindrical shells by using the GDQ method.

In view of the literature, it is found that the stability analysis of piezoelectric NTRC cylindrical shells is very limited, especially for piezoelectric FG-NTRC cylindrical shells. Most of the work were performed based on numerical methods, e.g., energy method [Ghorbanpour Arani et al. 2012a; 2012b; Mosallaie Barzoki et al. 2012; Ansari et al. 2016; Ninh 2018], GDQ method [Mosallaie Barzoki et al. 2013; Ghorbanpour Arani et al. 2014; SafarPour et al. 2019]. Analytical solutions were only reported by Salehi-Khojin and Jalili [2008], which was derived by the trial functions. Although the numerical approach could directly aid the engineering design, the analysis of data may be very time-consuming. In this case, analytical solutions could provide an efficient way to the rapid design and evaluation of such cylindrical shells.

Motivated by this, we employ a new Hamiltonian-based method [Wang and Qin 2007; Chen and Zhao 2009; Yao et al. 2009; Lim and Xu 2010; Sun et al. 2013; 2014a; 2014b; Li et al. 2015; Ni et al. 2017; 2018] to find exact solutions for buckling of piezoelectric FG-NTRC cylindrical shells under combined electro-thermo-mechanical loads. By introducing a total unknown vector, the high-order governing differential equations for buckling of the shell is reduced into a set of low-order ordinary equations. Thus, the buckling problem of the piezoelectric FG-NTRC shell is regarded as an eigenproblem in the symplectic space so that the exact solutions can be directly represented by the symplectic eigenfunctions. Unlike the single-formed solution obtained by the classical analytical treatments, the present solutions have five possible forms which highly depend on the geometrical parameters, circumference wave numbers, reinforcement nanotubes and their distribution patterns. Numerical examples are provided to reveal the effects of key influencing factors on the expressions of symplectic eigenfunctions and critical buckling stresses.

This paper is organized as follows. Following this introduction, modeling of piezoelectric FG-NTRC cylindrical shells under combined electro-thermo-mechanical loads is established. The basic equations are presented in Section 3. The Hamiltonian form of governing buckling equations and exact solutions are given in Sections 4 and 5, respectively. Numerical examples are provided in Section 6. Finally, the conclusions are summarized in Section 7.

2. Modeling of piezoelectric NTRC cylindrical shells

Consider a piezoelectric FG-NTRC cylindrical shell with external electric voltage θ_0, temperature field $T(z)$ and axial compression F in Figure 1 (left). The geometries are taken as length L, radius R and thickness h. It is referred to a shell coordinate system (x, θ, z) where x, θ and z are in the axial, circumferential and outward normal directions of the middle surface of shell. The displacements along x-, θ- and z- axes are specified by u, v and w, respectively.

The NTRC is made from a mixture of NTs and an isotropic matrix. Four distribution patterns of the NTs along the thickness direction are considered in the present study, as shown in Figure 1 (right). The corresponding volume fractions of NTs are as follows [Ghorbanpour Arani et al. 2016; Mohammadimehr et al. 2016]:

Uniformly distribution (UD):	$V_{NT} = V_{NT}^*,$	(1a)
FG-X:	$V_{NT} = 2(2|z|/h)V_{NT}^*,$	(1b)
FG-O:	$V_{NT} = 2(2 - 2|z|/h)V_{NT}^*,$	(1c)
FG-V:	$V_{NT} = (1 + 2z/h)V_{NT}^*,$	(1d)

where V_{NT}^* is total volume fraction of the NTs and it ranges from 0 to 0.5.

It is considered that the constituents of NTRC are orthotropic and homogeneous along the principal axis. The effective material properties of NTRC are evaluated by using the representative volume element based on micromechanical models. The mechanical, electrical and thermal properties are expressed as [Ghorbanpour Arani et al. 2016; Mosallaie Barzoki et al. 2012; Salehi-Khojin and Jalili 2008; Tan and

Tong 2001a; 2001b]:

$$c_{11} = \frac{c_{11}^{NT} c_{11}^{M}}{V_{NT}\, c_{11}^{M} + V_M\, c_{11}^{NT}}, \quad c_{12} = c_{11}\left(V_{NT}\, \frac{c_{12}^{NT}}{c_{11}^{NT}} + V_M\, \frac{c_{12}^{M}}{c_{11}^{M}} \right),$$

$$c_{22} = V_{NT}\, c_{22}^{NT} + V_M\, c_{22}^{M}, \quad c_{66} = \frac{c_{66}^{NT} c_{66}^{M}}{V_{NT}\, c_{66}^{M} + V_M\, c_{66}^{NT}}, \tag{2a}$$

$$e_{31} = c_{11}\left(V_{NT}\, \frac{e_{31}^{NT}}{c_{11}^{NT}} + V_M\, \frac{e_{31}^{M}}{c_{11}^{M}} \right), \quad e_{32} = V_{NT}\, e_{32}^{NT} + V_M\, e_{32}^{M}, \tag{2b}$$

$$\varepsilon_{11} = V_{NT}\, \varepsilon_{11}^{NT} + V_M\, \varepsilon_{11}^{M}, \quad \varepsilon_{22} = V_{NT}\, \varepsilon_{22}^{NT} + V_M\, \varepsilon_{22}^{M}, \quad \varepsilon_{33} = V_{NT}\, \varepsilon_{33}^{NT} + V_M\, \varepsilon_{33}^{M}, \tag{2c}$$

$$\beta_1 = V_{NT}\, \beta_1^{NT} + V_M\, \beta_1^{M}, \quad \beta_2 = V_{NT}\, \beta_2^{NT} + V_M\, \beta_2^{M}, \tag{2d}$$

$$p_3 = V_{NT}\, p_3^{NT} + V_M\, p_3^{M}, \tag{2e}$$

where V_M is the volume fractions of matrix which satisfies $V_{NT} + V_M = 1$; c_{11}^i, c_{12}^i, c_{22} and c_{66}^i are elasticity constants; e_{31}^i and e_{32}^i are piezoelectric constants; ε_{11}^i, ε_{22}^i and ε_{33}^i are dielectric constants; β_1^i and β_2^i are thermal moduli; p_3^i is pyroelectric constant; "$i = NT$" and "$i = M$" represent the NTs and matrix, respectively.
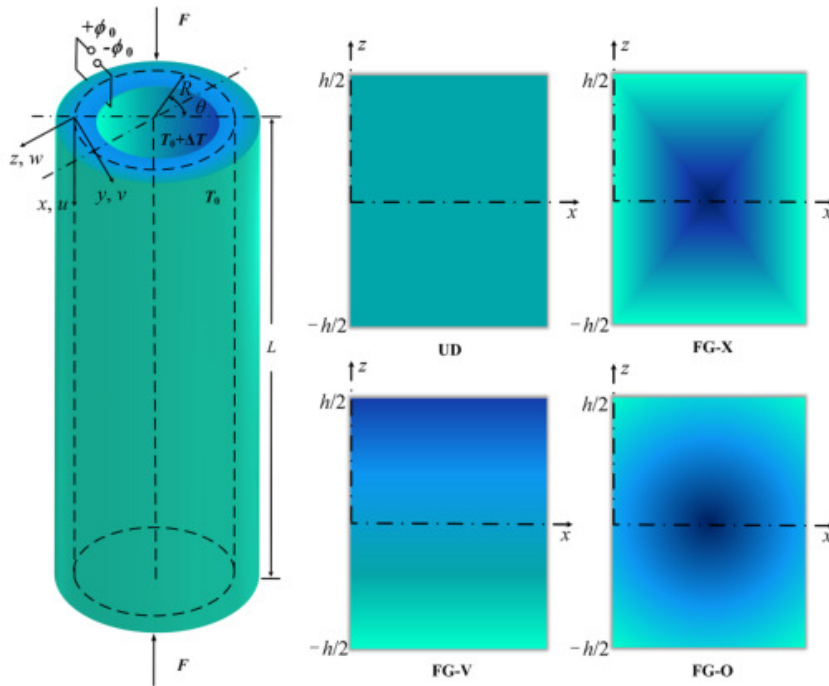

Figure 1. A piezoelectric NTRC cylindrical shell. Left: geometry of a piezoelectric NTRC cylindrical shell with thermal load, electric voltage and axial compression. Right: four distribution patterns of NTs.

3. Formulations of piezoelectric NTRC cylindrical shells

According to Reissner's shell theory [Leissa 1993], the strain components on the middle surface of the piezoelectric NTRC cylindrical shell are expressed as

$$\varepsilon_x = \frac{\partial u}{\partial x} - \frac{\partial^2 w}{\partial x^2} z, \tag{3a}$$

$$\varepsilon_\theta = \frac{1}{R}\frac{\partial v}{\partial \theta} + \frac{w}{R} - \frac{1}{R^2}\left(\frac{\partial^2 w}{\partial \theta^2} - \frac{\partial v}{\partial \theta}\right) z, \tag{3b}$$

$$\gamma_{x\theta} = \frac{\partial v}{\partial x} + \frac{1}{R}\frac{\partial u}{\partial \theta} - \frac{1}{R}\left(2\frac{\partial^2 w}{\partial \theta\,\partial x} - \frac{\partial v}{\partial x}\right) z. \tag{3c}$$

To simplify the manipulation, the electric potential which satisfies the Maxwell equation can be assumed as a combination of cosine and linear variation, i.e., [Wang 2002; Pietrzakowski 2008; Lang and Xuewu 2013; Ke et al. 2014; Mehralian et al. 2016a; Mehralian and Tadi Beni 2017b; 2018]

$$\tilde{\phi}(x, \theta, z) = -\cos(\beta z)\phi(x, \theta) + \frac{2z\phi_0}{h}, \tag{4}$$

where $\beta = \pi/h$; ϕ is electric potential induced by elastic deformation; ϕ_0 is the applied uniform electric voltage marked in Figure 1 (left).

The electric field $\boldsymbol{E} = \{E_x, E_\theta, E_z\}^{\mathrm{T}}$ are written as [Ke et al. 2014]

$$E_x = -\frac{\partial \tilde{\phi}}{\partial x} = \cos(\beta x)\frac{\partial \phi}{\partial x}, \tag{5a}$$

$$E_\theta = -\frac{1}{R+z}\frac{\partial \tilde{\phi}}{\partial \theta} = \frac{\cos(\beta z)}{R+z}\frac{\partial \phi}{\partial \theta}, \tag{5b}$$

$$E_z = -\frac{\partial \tilde{\phi}}{\partial z} = -\beta \sin(\beta z)\phi - \frac{2\phi_0}{h}. \tag{5c}$$

The thermo-electro-mechanical constitutive equation for piezoelectric cylindrical shell under the plane stress state is given by [Ke et al. 2014]

$$\begin{Bmatrix} \sigma_x \\ \sigma_\theta \\ \sigma_{x\theta} \end{Bmatrix} = \begin{bmatrix} c_{11} & c_{12} & 0 \\ c_{12} & c_{22} & 0 \\ 0 & 0 & c_{66} \end{bmatrix} \begin{Bmatrix} \varepsilon_x \\ \varepsilon_\theta \\ \gamma_{x\theta} \end{Bmatrix} - \begin{bmatrix} 0 & 0 & e_{31} \\ 0 & 0 & e_{32} \\ 0 & 0 & 0 \end{bmatrix} \begin{Bmatrix} E_x \\ E_\theta \\ E_z \end{Bmatrix} - \begin{Bmatrix} \beta_1 \\ \beta_2 \\ 0 \end{Bmatrix} T(z), \tag{6a}$$

$$\begin{Bmatrix} D_x \\ D_\theta \\ D_z \end{Bmatrix} = \begin{bmatrix} 0 & 0 & 0 \\ 0 & 0 & 0 \\ e_{31} & e_{32} & 0 \end{bmatrix} \begin{Bmatrix} \varepsilon_x \\ \varepsilon_\theta \\ \gamma_{x\theta} \end{Bmatrix} + \begin{bmatrix} \varepsilon_{11} & 0 & 0 \\ 0 & \varepsilon_{22} & 0 \\ 0 & 0 & \varepsilon_{33} \end{bmatrix} \begin{Bmatrix} E_x \\ E_\theta \\ E_z \end{Bmatrix} + \begin{Bmatrix} 0 \\ 0 \\ p_3 \end{Bmatrix} T(z), \tag{6b}$$

where σ_{ij} and D_i are stress and electric displacement components, respectively.

Integrating (6), the force, moment and generalized electric displacement resultants of the cylindrical shell are obtained as

$$\{N_x, N_\theta, N_{x\theta}\}^{\mathrm{T}} = \int_{-h/2}^{h/2} \{\sigma_x, \sigma_\theta, \sigma_{x\theta}\}^{\mathrm{T}} \, dz, \tag{7a}$$

$$\{M_x, M_\theta, M_{x\theta}\}^{\mathrm{T}} = \int_{-h/2}^{h/2} \{\sigma_x, \sigma_\theta, \sigma_{x\theta}\}^{\mathrm{T}} z \, dz, \tag{7b}$$

$$\{\Lambda_x, \Lambda_\theta, \Lambda_x\}^{\mathrm{T}} = \int_{-h/2}^{h/2} -R \left\{ \cos(\beta z) \, D_x, \frac{\cos(\beta z)}{R+z} D_\theta, \beta \sin(\beta z) \, D_z \right\}^{\mathrm{T}} dz. \tag{7c}$$

The relations between the shear forces and moments can be expressed as

$$Q_x = \frac{\partial M_x}{\partial x} + \frac{1}{R} \frac{\partial M_{x\theta}}{\partial \theta} \quad \text{and} \quad Q_\theta = \frac{\partial M_{x\theta}}{\partial x} + \frac{1}{R} \frac{\partial M_\theta}{\partial \theta}. \tag{8}$$

The prebuckling state can be considered as uniform deformation or axisymmetric deformation and has a significant effect only for a particularly short and thick cylindrical shell [Yamaki 1984; Teng 1996; Rotter 2014; Teng and Rotter 2014]. In the present study, since the displacement and angle of rotation are very small, the prebuckling state is assumed as a uniform deformation. When the external loads increase to a certain extent, another new equilibrium state will appear on the basis of the original equilibrium state under external disturbance. The bifurcation buckling of the structure occurs at this time, and the governing equation of linear buckling for the state of stability is established. The corresponding state variables can be divided into

$$\{u, v, w, \phi\} = \{u^0, v^0, w^0, \phi^0\} + \{u^1, v^1, w^1, \phi^1\}, \tag{9a}$$

$$\{E_x, E_\theta, E_z\} = \{E_x^0, E_\theta^0, E_z^0\} + \{E_x^1, E_\theta^1, E_z^1\}, \tag{9b}$$

$$\{D_x, D_\theta, D_z\} = \{D_x^0, D_\theta^0, D_z^0\} + \{D_x^1, D_\theta^1, D_z^1\}, \tag{9c}$$

$$\{N_x, N_\theta, N_{x\theta}\} = \{N_x^0, N_\theta^0, N_{x\theta}^0\} + \{N_x^1, N_\theta^1, N_{x\theta}^1\}, \tag{9d}$$

$$\{M_x, M_\theta, M_{x\theta}\} = \{M_x^0, M_\theta^0, M_{x\theta}^0\} + \{M_x^1, M_\theta^1, M_{x\theta}^1\}, \tag{9e}$$

$$\{\Lambda_x, \Lambda_\theta, \Lambda_{x\theta}\} = \{\Lambda_x^0, \Lambda_\theta^0, \Lambda_{x\theta}^0\} + \{\Lambda_x^1, \Lambda_x^1, \Lambda_{x\theta}^1\}, \tag{9f}$$

$$\{Q_x, Q_\theta\} = \{Q_x^0, Q_\theta^0\} + \{Q_x^1, Q_\theta^1\}, \tag{9g}$$

where the superscripts "0" and "1" correspond to the prebuckling quantities and infinitesimal increments. The corresponding resultant forces in prebuckling state can be obtained as $N_x^0 = N_e^0 + N_t^0 + N_m^0$ where $N_e^0 = -2 \int_{-h/2}^{h/2} e_{31} \phi_0 / h \, dz$, $N_t^0 = \int_{-h/2}^{h/2} \beta_1 T(z) \, dz$ and $N_m^0 = F/2\pi R$ represent the internal forces caused by external electric voltage, temperature rise and external axial compression, respectively.

Substituting (3) and (6) into (7), internal forces and generalized electric displacements for the state of stability can be simplified as

$$N_x^1 = A_{11}\frac{\partial u^1}{\partial x} + \frac{A_{12}}{R}\left(\frac{\partial v^1}{\partial \theta} + w^1\right) - B_{11}\frac{\partial^2 w^1}{\partial x^2} - \frac{B_{12}}{R^2}\left(\frac{\partial^2 w^1}{\partial \theta^2} - \frac{\partial v^1}{\partial \theta}\right), \tag{10a}$$

$$N_\theta^1 = A_{21}\frac{\partial u^1}{\partial x} + \frac{A_{22}}{R}\left(\frac{\partial v^1}{\partial \theta} + w^1\right) - B_{21}\frac{\partial^2 w^1}{\partial x^2} - \frac{B_{22}}{R^2}\left(\frac{\partial^2 w^1}{\partial \theta^2} - \frac{\partial v^1}{\partial \theta}\right), \tag{10b}$$

$$N_{x\theta}^1 = A_{66}\left(\frac{\partial v^1}{\partial x} + \frac{\partial u^1}{R\partial \theta}\right) - \frac{B_{66}}{R}\left(2\frac{\partial^2 w^1}{\partial x\,\partial \theta} - \frac{\partial v^1}{\partial x}\right), \tag{10c}$$

$$M_x^1 = B_{11}\frac{\partial u^1}{\partial x} + \frac{B_{12}}{R}\left(\frac{\partial v^1}{\partial \theta} + w^1\right) - D_{11}\frac{\partial^2 w^1}{\partial x^2} - \frac{D_{12}}{R^2}\left(\frac{\partial^2 w^1}{\partial \theta^2} - \frac{\partial v^1}{\partial \theta}\right) + E_{31}\phi^1, \tag{10d}$$

$$M_\theta^1 = B_{21}\frac{\partial u^1}{\partial x} + \frac{B_{22}}{R}\left(\frac{\partial v^1}{\partial \theta} + w^1\right) - D_{21}\frac{\partial^2 w^1}{\partial x^2} - \frac{D_{22}}{R^2}\left(\frac{\partial^2 w^1}{\partial \theta^2} - \frac{\partial v^1}{\partial \theta}\right) + E_{32}\phi^1, \tag{10e}$$

$$M_{x\theta}^1 = B_{66}\left(\frac{\partial v^1}{\partial x} + \frac{\partial u^1}{R\partial u}\right) - \frac{D_{66}}{R}\left(2\frac{\partial^2 w^1}{\partial x\,\partial \theta} - \frac{\partial v^1}{\partial x}\right), \tag{10f}$$

$$\Lambda_x^1 = -RX_{11}\frac{\partial \phi^1}{\partial x}, \tag{10g}$$

$$\Lambda_\theta^1 = -RX_{22}\frac{\partial \phi^1}{\partial \theta}, \tag{10h}$$

$$\Lambda_z^1 = RE_{31}\frac{\partial^2 w^1}{\partial x^2} + \frac{E_{32}}{R}\left(\frac{\partial^2 w^1}{\partial \theta^2} - \frac{\partial v^1}{\partial \theta}\right) + RX_{33}\phi^1, \tag{10i}$$

where

$$\{A_{ij}, B_{ij}, D_{ij}\} = \int_{-h/2}^{h/2} c_{ij}\{1, z, z^2\}\,dz \quad (i, j = 1, 2, 6),$$

are components of the extensional, coupling and bending stiffness, $A_{12} = A_{21}$, $B_{12} = B_{21}$ and $D_{12} = D_{21}$,

$$\{E_{31}, E_{32}\} = \int_{-h/2}^{h/2}\{e_{31}, e_{32}\}\,\beta z \sin(\beta z)\,dz, \quad X_{11} = \int_{-h/2}^{h/2}\varepsilon_{11}\cos^2(\beta z)\,dz,$$

$$X_{22} = \int_{-h/2}^{h/2}\varepsilon_{22}\frac{\cos^2(\beta z)}{(R+z)^2}\,dz, \qquad X_{33} = \int_{-h/2}^{h/2}\varepsilon_{33}\beta^2 \sin^2(\beta z)\,dz.$$

The governing equations for the state of stability can be obtained as [Ke et al. 2014]

$$\frac{\partial N_x^1}{\partial x} + \frac{\partial N_{x\theta}^1}{R\partial \theta} = 0, \qquad\qquad \frac{\partial N_{x\theta}^1}{\partial x} + \frac{\partial N_\theta^1}{R\partial \theta} + \frac{Q_\theta^1}{R} = 0, \tag{11a}$$

$$\frac{\partial Q_x^1}{\partial x} + \frac{\partial Q_\theta^1}{R\partial \theta} - \frac{N_\theta^1}{R} - N_x^0\frac{\partial^2 w^1}{\partial x^2} = 0, \quad \frac{\partial \Lambda_x^1}{\partial x} + \frac{\partial \Lambda_\theta^1}{\partial \theta} + \Lambda_z^1 = 0. \tag{11b}$$

Two types of end conditions at $x = 0$ and L are considered here [Chen et al. 1996; Hussein and Heyliger 1998; Saviz et al. 2007; Ke et al. 2014; Sun et al. 2016], i.e.,

Clamped (C):
$$u^1 = v^1 = w^1 = \frac{\partial w^1}{\partial x} = \phi^1 = 0, \tag{12a}$$

Simply supported (S):
$$\frac{\partial u^1}{\partial x} = v^1 = w^1 = M_x^1 = \phi^1 = 0. \tag{12b}$$

4. Governing equations in Hamiltonian system

To obtain the analytical solutions of (11), the Hamiltonian description is introduced here. Define $\boldsymbol{q}$ and $\boldsymbol{p}$ as the original vector and its dual vector in the Hamiltonian system, respectively. The original vector is assumed as a vector consisting of displacements, angle of rotation and electric potential, i.e.,

$$\boldsymbol{q} = \{q_1, q_2, q_3, q_4, q_5\}^{\mathrm{T}} = \{u^1, v^1, w^1, \theta_\theta^1, \phi^1\}^{\mathrm{T}}, \tag{13}$$

where ϕ_θ^1 is the angle of rotation,

$$\theta_\theta^1 = \frac{v^1}{R} - \frac{1}{R}\frac{\partial w^1}{\partial \theta}. \tag{14}$$

The Lagrangian density function L_C is introduced as [Ke et al. 2014]

$$
\begin{aligned}
L_C = {} & -\frac{R}{2}\int_{-h/2}^{h/2}\left(D_x^1 E_x^1 + D_\theta^1 E_\theta^1 + D_z^1 E_z^1\right)dz \\
& + \frac{R}{2}\left[A_{11}\left(\frac{\partial u^1}{\partial x}\right)^2 + A_{22}\left(\frac{\dot{v}^1}{R} + \frac{w^1}{R}\right)^2 + 2A_{12}\frac{\partial u^1}{\partial x}\left(\frac{\dot{v}^1}{R} + \frac{w^1}{R}\right) + A_{66}\left(\frac{\partial v^1}{\partial x} + \frac{\dot{u}^1}{R}\right)^2 \right. \\
& \quad - 2\frac{B_{66}}{R}\left(\frac{\partial v^1}{\partial x} + \frac{\dot{u}^1}{R}\right)\left(2\frac{\partial \dot{w}^1}{\partial x} - \frac{\partial v^1}{\partial x}\right) - 2B_{11}\frac{\partial u^1}{\partial x}\frac{\partial^2 w^1}{\partial x^2} \\
& \quad - 2B_{12}\left(\frac{\dot{v}^1}{R} + \frac{w^1}{R}\right)\frac{\partial^2 w^1}{\partial x^2} + 2\frac{B_{12}}{R}\frac{\partial u^1}{\partial x}\dot{\theta}_\theta^1 + 2\frac{B_{22}}{R}\left(\frac{\dot{v}^1}{R} + \frac{w^1}{R}\right)\dot{\theta}_\theta^1 \\
& \quad \left. + D_{11}\left(\frac{\partial^2 w^1}{\partial x^2}\right)^2 - 2\frac{D_{12}}{R}\frac{\partial^2 w^1}{\partial x^2}\dot{\theta}_\theta^1 + \frac{D_{22}}{R}\left(\dot{\theta}_\theta^1\right)^2 + \frac{D_{66}}{R}\left(2\frac{\partial \dot{w}^1}{\partial x} - \frac{\partial v^1}{\partial x}\right)^2\right] \\
& + \left[2B_{66}\left(\frac{\partial \dot{u}^1}{R\partial x} + \frac{\partial^2 v^1}{\partial x^2}\right) + \frac{B_{22}}{R^2}\left(\ddot{v}^1 + v^1 - R\theta_\theta^1\right) + B_{12}\frac{\partial \dot{u}^1}{R\partial x}\right. \\
& \quad \left. - D_{12}\frac{\partial^2 \dot{w}^1}{R\partial x^2} + \frac{D_{22}}{R^2}\ddot{\theta}_\theta^1 + 2D_{66}\left(2\frac{\partial^2 \theta_\theta^1}{\partial x^2} - \frac{\partial^2 v^1}{R\partial x^2}\right)\right]\left(\dot{w}^1 - v^1 + R\theta_\theta^1\right), \tag{15}
\end{aligned}
$$

where $(\dot{\ }) = \partial(\ )/\partial\theta$.

The corresponding dual vector $\boldsymbol{p}$ can be obtained by (15)

$$\boldsymbol{p} = \frac{\delta L_C}{\delta \dot{\boldsymbol{q}}} = \{p_1, p_2, p_3, p_4, p_5\}^{\mathrm{T}} = \left\{N_{x\theta}^1, N_\theta^1, V_\theta^1, M_\theta^1, \Lambda_\theta^1\right\}^{\mathrm{T}}, \tag{16}$$

where equivalent shear forces V_θ^1 can be expressed by

$$V_\theta^1 = Q_\theta^1 + \frac{\partial M_{x\theta}^1}{\partial x}. \tag{17}$$

From (14), we have

$$\dot{w}^1 = v^1 - R\theta_\theta^1. \tag{18}$$

Substituting (18) into (10), we have

$$\dot{u}^1 = \left(\frac{B_{66}}{A_{66}} - R\right)\frac{\partial v^1}{\partial x} - 2R\frac{B_{66}}{A_{66}}\frac{\partial \theta_\theta^1}{\partial x} + \frac{R}{A_{66}}N_{x\theta}^1, \tag{19}$$

$$\dot{v}^1 = R\frac{\kappa_3}{\kappa_2}\frac{\partial u^1}{\partial x} + R\frac{\kappa_5}{\kappa_2}\frac{\partial^2 w^1}{\partial x^2} - w^1 + R\frac{D_{22}}{\kappa_2}N_\theta^1 - R\frac{B_{22}}{\kappa_2}M_\theta^1 + R\frac{B_{22}E_{32}}{\kappa_2}\phi^1, \tag{20}$$

$$\dot{\theta}_\theta^1 = -R\frac{\kappa_4}{\kappa_2}\frac{\partial u^1}{\partial x} + R\frac{\kappa_6}{\kappa_2}\frac{\partial^2 w^1}{\partial x^2} - R\frac{B_{22}}{\kappa_2}N_\theta^1 + R\frac{A_{22}}{\kappa_2}M_\theta^1 - R\frac{A_{22}E_{32}}{\kappa_2}\phi^1, \tag{21}$$

$$\dot{\phi}^1 = -\frac{1}{RX_{22}}\Lambda_\theta^1. \tag{22}$$

Substituting (10), (18), (20) and (21) into (11), we have

$$\dot{N}_{x\theta}^1 = R\left(\frac{\kappa_{10}}{D_{22}\kappa_2}\frac{\partial^2 u^1}{\partial x^2} + \frac{\kappa_{11}}{D_{22}\kappa_2}\frac{\partial^3 w^1}{\partial x^3} + \frac{\kappa_3}{\kappa_2}\frac{\partial N_\theta^1}{\partial x} - \frac{\kappa_4}{\kappa_2}\frac{\partial M_\theta^1}{\partial x} + E_{32}\frac{\kappa_4}{\kappa_2}\frac{\partial \phi^1}{\partial x}\right). \tag{23}$$

Substituting (10), (17) and (18) into (11), we have

$$\dot{N}_\theta^1 = -\frac{\kappa_9}{R}\frac{\partial^2 v^1}{\partial x^2} + 2\kappa_9\frac{\partial^2 \theta_\theta^1}{\partial x^2} + \left(\frac{B_{66}}{A_{66}} - R\right)\frac{\partial N_{x\theta}^1}{\partial x} - V_\theta^1. \tag{24}$$

Substituting (10), (17), (18), (20) and (21) into (11), we have

$$\dot{V}_\theta^1 = -R\left[\frac{\kappa_{11}}{D_{22}\kappa_2}\frac{\partial^3 u^1}{\partial x^3} + \frac{\kappa_{12}}{D_{22}\kappa_2}\frac{\partial^4 w^1}{\partial x^4} + \frac{\kappa_5}{\kappa_2}\frac{\partial^2 N_\theta^1}{\partial x^2} + \frac{\kappa_6}{\kappa_2}\frac{\partial^2 M_\theta^1}{\partial x^2} + \left(E_{31} - \frac{\kappa_6}{\kappa_2}E_{32}\right)\frac{\partial^2 \phi^1}{\partial x^2}\right]$$
$$+ N_\theta^1 + RN_x^0\frac{\partial^2 w^1}{\partial x^2}. \tag{25}$$

Substituting (10), (17), (18) and (19) into (8), we have

$$\dot{M}_\theta^1 = 2\kappa_9\frac{\partial^2 v^1}{\partial x^2} - 4R\kappa_9\frac{\partial^2 \theta_\theta^1}{\partial x^2} - 2R\frac{B_{66}}{A_{66}}\frac{\partial N_{x\theta}^1}{\partial x} + RV_\theta^1. \tag{26}$$

Substituting (10) into (11), we have

$$\dot{\Lambda}_\theta^1 = -R\left[E_{32}\frac{\kappa_4}{\kappa_2}\frac{\partial u^1}{\partial x} + \left(E_{31} - \frac{\kappa_6}{\kappa_2}E_{32}\right)\frac{\partial^2 w^1}{\partial x^2} + \frac{E_{32}B_{22}}{\kappa_2}N_\theta^1 - \frac{E_{32}A_{22}}{\kappa_2}M_\theta^1 - X_{11}\frac{\partial^2 \phi^1}{\partial x^2}\right.$$
$$\left. + \left(X_{33} + \frac{A_{22}E_{32}^2}{\kappa_2}\right)\phi^1\right]. \tag{27}$$

where $\kappa_1 = A_{11}D_{22} - B_{12}^2$, $\kappa_2 = A_{22}D_{22} - B_{22}^2$, $\kappa_3 = B_{22}B_{12} - A_{12}D_{22}$, $\kappa_4 = A_{22}B_{12} - A_{12}B_{22}$, $\kappa_5 = B_{12}D_{22} - B_{22}D_{12}$, $\kappa_6 = A_{22}D_{12} - B_{22}B_{12}$, $\kappa_7 = B_{12}D_{12} - B_{11}D_{22}$, $\kappa_8 = D_{12}^2 - D_{11}D_{22}$, $\kappa_9 = (A_{66}D_{66} - B_{66}^2)/A_{66}$, $\kappa_{10} = \kappa_3^2 - \kappa_1\kappa_2$, $\kappa_{11} = \kappa_3\kappa_5 - \kappa_7\kappa_2$ and $\kappa_{12} = \kappa_8\kappa_2 + \kappa_5^2$.

In view of (18)–(27), the Hamiltonian governing equations can be represented in a matrix form of

$$\dot{\boldsymbol{\psi}} = \boldsymbol{H}\boldsymbol{\psi}, \tag{28}$$

where $\boldsymbol{\psi} = \{\boldsymbol{q}^{\mathrm{T}}, \boldsymbol{p}^{\mathrm{T}}\}^{\mathrm{T}}$ is a total unknown vector; $\boldsymbol{H}$ is the Hamiltonian operator matrix in Appendix A.

The associated end conditions (12) are rewritten in the Hamiltonian form:

C: $$q_1 = q_2 = q_3 = \frac{\partial q_3}{\partial x} = q_5 = 0, \tag{29a}$$

S: $$\frac{\partial q_1}{\partial x} = q_2 = q_3 = \frac{\kappa_{11}}{D_{22}\kappa_2}\frac{\partial q_1}{\partial x} + \frac{\kappa_{12}}{D_{22}\kappa_2}\frac{\partial^2 q_3}{\partial x^2} + E_{31}q_5 + \frac{\kappa_5}{\kappa_2}p_2 + \frac{\kappa_6}{\kappa_2}p_4 = q_5 = 0. \tag{29b}$$

5. Symplectic eigenvalue problem and buckling equation

According to the Hamiltonian matrix, the method of separation of variables is available to solve the governing equation (28) [Lim and Xu 2010]. Assuming that $\boldsymbol{\psi}(x, \theta) = \boldsymbol{\eta}(x)e^{\mu\theta}$, the eigenvalue equation for (28) has the form of

$$\boldsymbol{H}\boldsymbol{\eta}_n = \mu\boldsymbol{\eta}_n, \tag{30}$$

where $\mu = n\mathrm{i}$ ($n = 0, \pm 1, \pm 2, \dots$) and $\boldsymbol{\eta}(x)$ are the symplectic eigenvalues and eigenfunctions, respectively. It is worthy of note that the eigenfunctions $\boldsymbol{\eta}_n$ can be divided into two groups: zero eigenfunctions $\boldsymbol{\eta}_0$ with $\mu = 0$ and nonzero eigenfunctions $\boldsymbol{\eta}_n$ with $\mu \neq 0$. The physical interpretations of $\boldsymbol{\eta}_0$ and $\boldsymbol{\eta}_n$ are the axisymmetric and nonaxisymmetric buckling solutions of the piezoelectric cylindrical shell, respectively. Thus, the zero eigenfunctions and nonzero eigenfunctions are solved separately.

5.1. *Zero eigenfunction.* Considering zero eigenfunctions, the eigenvalue equation has the form of $\boldsymbol{H}\boldsymbol{\eta}_0^{(1)} = 0$. In this case, characteristic equation is

$$\lambda^{10} + \xi_1^{(0)}\lambda^8 + \xi_2^{(0)}\lambda^6 + \xi_3^{(0)}\lambda^4 + \xi_4^{(0)}\lambda^2 + \xi_5^{(0)} = 0, \tag{31}$$

in which ξ_i^0 ($i = 1, 2, \dots, 5$) are the functions of compressive buckling load N_x^0, which are elaborated in Appendix B.

The root of (31) are $\lambda_{1,2} = \pm \mathrm{i}\alpha_1$, $\lambda_{3,4} = \pm \mathrm{i}\alpha_2$, $\lambda_{5,6} = \pm \alpha_3$, $\lambda_7 = \lambda_8 = \lambda_9 = \lambda_{10} = 0$. Thus, the zero eigenfunctions can be represented by

Case I ($\mu = 0$):
$$\boldsymbol{\eta}_0^{(1)} = \boldsymbol{c}_1 \cos(\alpha_1 x) + \boldsymbol{c}_2 \sin(\alpha_1 x) + \boldsymbol{c}_3 \cos(\alpha_2 x) + \boldsymbol{c}_4 \sin(\alpha_2 x) + \boldsymbol{c}_5 e^{\alpha_3 x} + \boldsymbol{c}_6 e^{-\alpha_3 x}$$
$$+ \boldsymbol{c}_7 + \boldsymbol{c}_8 x + \boldsymbol{c}_9 x^2 + \boldsymbol{c}_{10} x^3, \tag{32}$$

where $\boldsymbol{c}_j = \{c_j^1, c_j^2, \dots, c_j^{10}\}^{\mathrm{T}}$ ($j = 1, 2, \dots, 10$) are undetermined coefficient vectors. The physical interpretations of (32) are the axisymmetric buckling solutions of the piezoelectric cylindrical shell.

5.2. *Nonzero eigenfunction.* Considering nonzero eigenfunctions, the characteristic equation obtained from the eigenvalue equation $(\boldsymbol{H} - \mu \boldsymbol{I})\boldsymbol{\eta}_n = 0$ is written as

$$\lambda^{10} + \xi_1 \lambda^8 + \xi_2 \lambda^6 + \xi_3 \lambda^4 + \xi_4 \lambda^2 + \xi_5 = 0, \tag{33}$$

where, ξ_i $(i = 1, 2, \ldots, 5)$ are the functions of compressive buckling load and are elaborated in Appendix C. The symplectic eigenfunctions can be expressed by

$$\boldsymbol{\eta}_n = \sum_{i=1}^{10} \boldsymbol{c}_i \, e^{\lambda_i x}, \tag{34}$$

where λ_i $(i = 1, 2, \ldots, 10)$ are the roots of (33); $\boldsymbol{c}_j = \{c_j^1, c_j^2, \ldots, c_j^{10}\}^{\mathrm{T}}$ $(j = 1, 2, \ldots, 10)$ are undetermined coefficient vectors. Here, it should be pointed out that there are only ten independent coefficients. To simplify the manipulation, $\boldsymbol{c}^1 = \{c_1^1, c_2^1, \ldots, c_{10}^1\}$ are chosen as the independent coefficients. Therefore, $\boldsymbol{c}^k = \{c_1^k, c_2^k, \ldots, c_{10}^k\}$ $(k = 2, 3, \ldots, 10)$ can be represented by $\boldsymbol{c}^1$.

According to λ and μ, the expressions of eigenfunction (34) can be grouped into five categories:

Case II $(\mu = \pm \mathrm{i})$: $\lambda_{1,2} = \pm \mathrm{i}\alpha_1$, $\lambda_{3,4} = \pm \mathrm{i}\alpha_2$, $\lambda_{5,6} = \pm \mathrm{i}\alpha_3$, $\lambda_{7,8} = \pm \alpha_4$, $\lambda_{9,10} = 0$,

$$\begin{aligned}\boldsymbol{\eta}_n^{(2)} = \boldsymbol{c}_1 \cos(\alpha_1 x) + \boldsymbol{c}_2 \sin(\alpha_1 x) + \boldsymbol{c}_3 \cos(\alpha_2 x) + \boldsymbol{c}_4 \sin(\alpha_2 x) + \boldsymbol{c}_5 \cos(\alpha_3 x) + \boldsymbol{c}_6 \sin(\alpha_3 x) \\ + \boldsymbol{c}_7 e^{\alpha_4 x} + \boldsymbol{c}_8 e^{-\alpha_4 x} + \boldsymbol{c}_9 + \boldsymbol{c}_{10} x, \end{aligned} \tag{35}$$

Case III $(\mu = \pm \mathrm{i})$: $\lambda_{1,2} = \pm \mathrm{i}\alpha_1$, $\lambda_{3,4} = \pm \alpha_2$, $\lambda_{5,6} = \pm \alpha_3$, $\lambda_{7,8} = \pm \alpha_4$, $\lambda_{9,10} = 0$,

$$\boldsymbol{\eta}_n^{(3)} = \boldsymbol{c}_1 \cos(\alpha_1 x) + \boldsymbol{c}_2 \sin(\alpha_1 x) + \boldsymbol{c}_3 e^{\alpha_2 x} + \boldsymbol{c}_4 e^{-\alpha_2 x} + \boldsymbol{c}_5 e^{\alpha_3 x} + \boldsymbol{c}_6 e^{-\alpha_3 x} + \boldsymbol{c}_7 e^{\alpha_4 x} + \boldsymbol{c}_8 e^{-\alpha_4 x} + \boldsymbol{c}_9 + \boldsymbol{c}_{10} x, \tag{36}$$

Case IV $(\mu \neq \pm \mathrm{i})$: $\lambda_{1,2} = \pm \mathrm{i}\alpha_1$, $\lambda_{3,4} = \pm \mathrm{i}\alpha_2$, $\lambda_{5,6} = \pm \alpha_3$, $\lambda_{7,8} = \pm(\alpha_4 + \mathrm{i}\alpha_5)$, $\lambda_{9,10} = \pm(\alpha_4 - \mathrm{i}\alpha_5)$,

$$\begin{aligned}\boldsymbol{\eta}_n^{(4)} = \boldsymbol{c}_1 \cos(\alpha_1 x) + \boldsymbol{c}_2 \sin(\alpha_1 x) + \boldsymbol{c}_3 \cos(\alpha_2 x) + \boldsymbol{c}_4 \sin(\alpha_2 x) + \boldsymbol{c}_5 e^{\alpha_3 x} + \boldsymbol{c}_7 e^{\alpha_4 x} \cos(\alpha_5 x) \\ + \boldsymbol{c}_8 e^{\alpha_4 x} \sin(\alpha_5 x) + \boldsymbol{c}_9 e^{-\alpha_4 x} \cos(\alpha_5 x) + \boldsymbol{c}_{10} e^{-\alpha_4 x} \sin(\alpha_5 x), \end{aligned} \tag{37}$$

Case V $(\mu \neq \pm \mathrm{i})$: $\lambda_{1,2} = \pm \mathrm{i}\alpha_1$, $\lambda_{3,4} = \pm \mathrm{i}\alpha_2$, $\lambda_{5,6} = \pm \alpha_3$, $\lambda_{7,8} = \pm \alpha_4$, $\lambda_{9,10} = \pm \alpha_5$,

$$\begin{aligned}\boldsymbol{\eta}_n^{(5)} = \boldsymbol{c}_1 \cos(\alpha_1 x) + \boldsymbol{c}_2 \sin(\alpha_1 x) + \boldsymbol{c}_3 \cos(\alpha_2 x) + \boldsymbol{c}_4 \sin(\alpha_2 x) + \boldsymbol{c}_5 e^{\alpha_3 x} + \boldsymbol{c}_6 e^{-\alpha_3 x} + \boldsymbol{c}_7 e^{\alpha_4 x} \\ + \boldsymbol{c}_8 e^{-\alpha_4 x} + \boldsymbol{c}_9 e^{\alpha_5 x} + \boldsymbol{c}_{10} e^{-\alpha_5 x}, \end{aligned} \tag{38}$$

Case VI $(\mu \neq \pm \mathrm{i})$: $\lambda_{1,2} = \pm \mathrm{i}\alpha_1$, $\lambda_{3,4} = \pm \mathrm{i}\alpha_2$, $\lambda_{5,6} = \pm \mathrm{i}\alpha_3$, $\lambda_{7,8} = \pm \mathrm{i}\alpha_4$, $\lambda_{9,10} = \pm \alpha_5$,

$$\begin{aligned}\boldsymbol{\eta}_n^{(6)} = \boldsymbol{c}_1 \cos(\alpha_1 x) + \boldsymbol{c}_2 \sin(\alpha_1 x) + \boldsymbol{c}_3 \cos(\alpha_2 x) + \boldsymbol{c}_4 \sin(\alpha_2 x) + \boldsymbol{c}_5 \cos(\alpha_3 x) + \boldsymbol{c}_6 \sin(\alpha_3 x) \\ + \boldsymbol{c}_7 \cos(\alpha_4 x) + \boldsymbol{c}_8 \sin(\alpha_4 x) + \boldsymbol{c}_9 e^{\alpha_5 x} + \boldsymbol{c}_{10} e^{-\alpha_5 x}, \end{aligned} \tag{39}$$

where α_i $(i = 1, 2, \ldots, 5)$ are determined by (33). These nonzero eigenfunctions $\boldsymbol{\eta}_n^{(i)}$ $(i = 1, 2, \ldots, 5)$ represent the nonaxisymmetric buckling solutions of the piezoelectric FG-NTRC cylindrical shell.

Buckling equations and buckling mode shape functions can be determined by means of eigenfunctions $\boldsymbol{\eta}$ and end conditions. Substituting (35)–(39) into (29), one has $[\boldsymbol{\varsigma}]_{10 \times 10}(\boldsymbol{c}^1)^{\mathrm{T}} = 0$. For nontrivial solutions, the determinant of the coefficient matrix of $\boldsymbol{\varsigma}$ should vanish. Thus, the compressive buckling loads $N_{mn} = N_m^0$ are the roots of $|\boldsymbol{\varsigma}| = 0$. The buckling stresses is determined as $\sigma_{mn} = N_{mn}/h$, where m and n are the axial wave numbers and circumference wave numbers, respectively. The smallest value of σ_{mn} is the critical buckling stress σ_{cr}. The analytical buckling mode shape functions q_1, q_2 and q_3 can be obtained by substituting the eigenvalues into the corresponding eigenfunctions.

6. Numerical examples and discussion

6.1. *Validations.* Since no available critical buckling load of piezoelectric FG-NTRC cylindrical shells is reported in the open literature, a simply supported piezoelectric FG cylindrical shell made of BaTiO$_3$/PZT-5A or BaTiO$_3$ /PZT-4 is considered to verify the accuracy of the proposed method. The material properties for PZT-5A, PZT-4 and BaTiO$_3$ are taken as those in [Dong and Wang 2007; Sheng and Wang 2010]. The effective material properties P vary continuously in the thickness direction and can be expressed as $P(z) = (P_o - P_i)(1/2 + z/h)^k + P_i$ where k is the volume fraction exponent, P_o and P_i denote the property of the outer and inner surface of the shell, respectively. The nondimensional buckling load is defined as N_{cr}/N_{ocr} where

$$N_{ocr} = \frac{Eh^2}{R\sqrt{3(1 - \nu^2)}}.$$

In the following numerical examples, a uniform temperature field is considered so that the temperature through the shell thickness rises uniformly by a certain amount $T(z) = \Delta T$. Variations of buckling loads for $m = n = 1$ versus k are plotted in Figure 2 with $L/R = 1$, $h/R = 0.01$, $N_m^0 = 0.2N_{ocr}$, $\phi_0 = 200$ V and $\Delta T = 200$ K. It can be seen that the trend of the present results are consistent with those reported by Sheng and Wang [2010] with minor errors. The errors are mainly caused by the difference of shell theories. The present results were obtained by Reissner's shell theory while the reference data were obtained by the first-order shear deformation theory. Furthermore, the relation between the buckling temperature rise for $m = n = 1$ and the electric voltage are shown in Figure 3 with $L/R = 1$, $h/R = 0.002$, $N_m^0 = 0.5N_{ocr}$ and $k = 1$. The present method again produces good agreement with the treatment in reference [Sheng and Wang 2010].
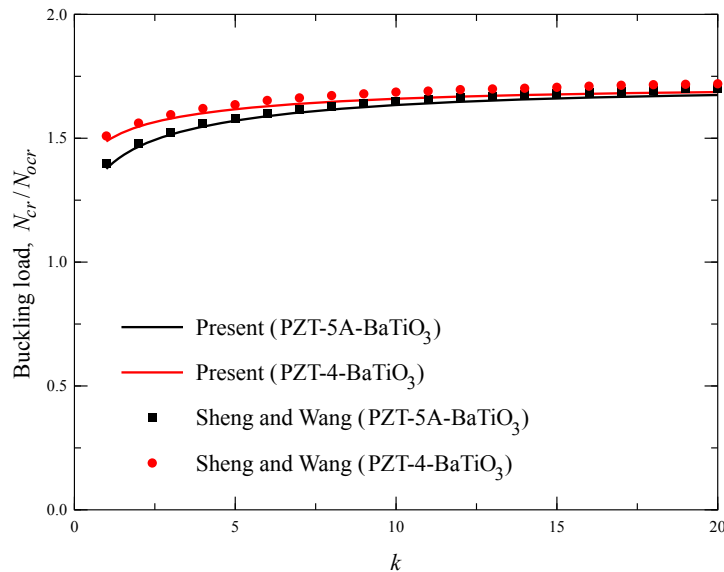

Figure 2. Comparison of the dimensionless buckling loads for S-S piezoelectric FG cylindrical shells with different volume fraction exponent k.
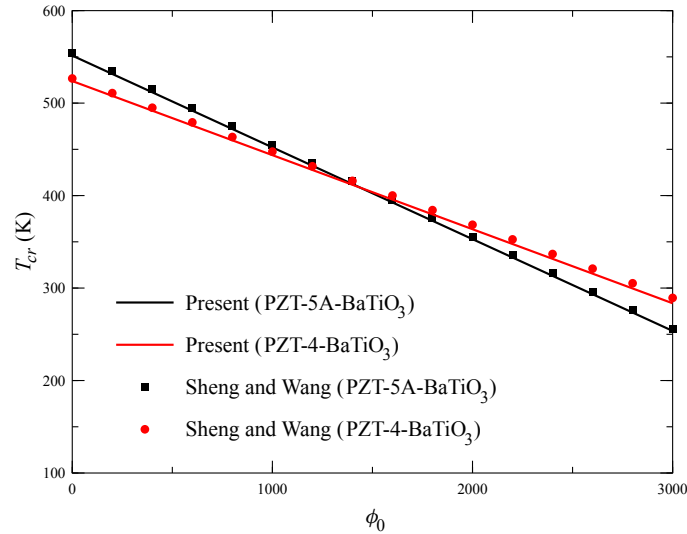
Figure 3. Comparison of the buckling temperature rise for S-S piezoelectric FG cylindrical shells with different ϕ_0.

For a further verification, the present results are compared with those obtained by high-order shear deformation theory (HSDT). The critical buckling stresses of a clamped isotropic piezoelectric cylindrical shell made of PZT-A or PZT-B without electric voltage and temperature rise are computed and tabulated in Table 1. The material properties are selected as those in [Sun et al. 2016]. It is observed that the present data obtained by Ressiner's shell theory are in accordance with those of HSDT [Sun et al. 2016] with a maximum error 2.86%. The errors are mainly caused by the difference of shell theories. The critical buckling loads predicted by the HSDT are usually less than the Ressiner's shell theory when the shell is relatively thick.

	$h/R = 1/30$	$h/R = 1/35$	$h/R = 1/40$	$h/R = 1/45$	$h/R = 1/50$
	$L/R = 1$				
Sun et al. (PZT-A)	1399.56	1199.57	1040.04	907.554	810.386
Present (PZT-A)	1433.91	1209.92	1043.43	913.969	808.000
Sun et al. (PZT-B)	1705.41	1447.32	1271.47	1120.34	997.118
Present (PZT-B)	1739.21	1481.68	1281.90	1110.33	991.122
	$L/R = 4$				
Sun et al. (PZT-A)	1281.11	1098.76	962.878	855.604	770.723
Present (PZT-A)	1317.75	1106.98	965.451	849.869	766.702
Sun et al. (PZT-B)	1565.56	1325.56	1159.39	1031.84	929.486
Present (PZT-B)	1607.89	1354.65	1153.65	1027.62	930.291

Table 1. Comparison of the critical buckling stresses (MPa) for a piezoelectric cylindrical shell with different L/R and h/R.

6.2. *Discussion on symplectic eigenfunctions.* In the existing literature, analytical analyses for buckling of piezoelectric cylindrical shells were usually performed by the inverse or semiinverse methods under the classical Lagrangian system. Analytical solutions were obtained by introducing some trial functions (e.g., trigonometric functions). Consequently, the obtained solutions highly depend on the expressions of the predetermined functions. To overcome the above limitation of classical analytical treatments, the present study proposed a rigorous method for buckling of piezoelectric FG-NTRC shells under the Hamiltonian system. The obtained analytical solutions are directly expressed in terms of symplectic eigenfunctions without any trial functions. It is interesting to find from Section 5 that there exist five cases of symplectic eigenfunctions ((35)–(39)) for buckling of the shell, which implies the analytical solutions may have five possible forms. To reveal the effects of key influencing parameters on the expressions of symplectic eigenfunctions, a piezoelectric FG-NTRC cylindrical shell with $R = 0.1$ m, $V_{NT}^* = 0.2$, $\phi_0 = 10000$ V and $\Delta T = 10$ K is considered in this section. The material properties of CNT, BNNT and polyvinylidene fluoride (PVDF) are tabulated in Table 2 [Mosallaie Barzoki et al. 2012; Mohammadimehr et al. 2016]. The buckling stresses, cases of symplectic eigenfunctions and their characteristic roots for three end conditions, various circumference wave number n, length L/R, thickness h/R, four distribution patterns of NTs and two kinds of reinforcement nanofiller are tabulated in tables 3–7.

From Table 3, it is clear that the end conditions do not affect the case of symplectic eigenfunctions regardless of circumference wave number n. It is also noted that the circumference wave number n has a significant influence on the case of symplectic eigenfunctions when n is small. However, the symplectic eigenfunctions always belong to Case V when n is large enough. Tables 4 and 5 present the buckling stresses, cases of symplectic eigenfunctions and their characteristic roots for various L/R and h/R. It is observed that the case of symplectic eigenfunctions have relations with the length and thickness of the shell when n is small. To further illustrate this, the variations of buckling stresses versus L/R and h/R with different n are plotted in figures 4 and 5. The influence of the reinforcement nanotubes (NT) and their distribution patterns on the case of symplectic eigenfunctions are investigated in tables 6 and 7, respectively. It is found that the piezoelectric FG-NTRC cylindrical shell with different reinforcement NTs and distribution patterns of NTs may produce different cases of symplecitc eigenfunctions when n is small.

Property	CNT	BNNT	PVDF
c_{11} (GPa)	5824.9	2035	238.24
c_{22} (GPa)	7303.7	2035	23.6
c_{12} (GPa)	1019.37	692	3.98
c_{66} (GPa)	1944.5	672	6.43
e_{31} (C/m^2)	0	0.95	-0.135
e_{32} (C/m^2)	0	-0.45	-0.145
$\varepsilon_{11} = \varepsilon_{22} = \varepsilon_{33}$ (10^{-9} C/Vm)	0	0.17708	11.068
β_1 (10^6 N K^{-1} m^{-2})	25.413	2.857	17.198
β_2 (10^6 N K^{-1} m^{-2})	41.272	2.051	1.958

Table 2. Material properties of BNNT, CNT and PVDF.

n	Eigensolution	Characteristic roots					σ_{mn} (MPa)
		C-C					
0	Case I	31.8519i	25.6692i	347.781	0	0	3513.36
1	Case II	28.4520i	22.2538i	0.135052i	347.783	0	3096.72
2	Case VI	12.3684i	5.79333i	3.23354i	0.193372i	347.787	1843.09
5	Case V	9.83078i	4.04971i	0.852275	66.0224	347.817	391.08
10	Case V	16.2447i	10.2467i	1.65614	134.083	347.925	746.39
		C-S					
0	Case I	30.1889i	27.0832i	347.781	0	0	3450.14
1	Case II	26.8361i	23.7118i	0.133366i	347.783	0	3047.35
2	Case VI	11.0384i	8.09206i	2.58624i	0.193946i	347.787	1836.50
5	Case V	8.01563i	4.96564i	0.852544	66.0167	347.817	339.36
10	Case V	14.5183i	11.4651i	1.65615	134.083	347.925	687.53
		S-S					
0	Case I	28.9171i	28.2743i	347.781	0	0	3429.71
1	Case II	25.3615i	25.1327i	0.132797i	347.783	0	3030.60
2	Case VI	9.90976i	9.42478i	2.47125i	0.194116i	347.787	1834.56
5	Case V	6.33423i	6.28319i	0.852649	66.0145	347.817	319.43
10	Case V	13.2460i	12.5664i	1.65615	134.083	347.925	667.97

Table 3. Buckling stresses, cases of symplectic eigenfunctions and characteristic roots for a piezoelectric FG-NTRC cylindrical shell reinforced by CNTs with different end conditions (FG-O, $m = 1$, $L/R = 1$, $h/R = 0.01$).

From tables 4–7, it is worth to note that the influences of geometrical parameters, reinforcement NTs and their distribution patterns on the case of symplectic eigenfunctions only occur under the conditions of a small circumference wave number n. In other words, analytical solutions for buckling of the piezoelectric FG-NTRC cylindrical shell have a unique expression consisting of Case V symplectic eigenfunctions when n is large enough. The observations explain the reasons for the use of single-formed trial functions in the classical analytical method. In the buckling analysis of cylindrical shells, the circumference wave number n for the critical buckling stress usually decreases with the increase of L/R [Yamaki 1984]. The length of shells in most of theoretical studies usually selected less than 10 (e.g., [Mirzavand and Eslami 2007; Mirzavand and Eslami 2011; Salehi-Khojin and Jalili 2008]) so that n for the critical buckling stress is larger than 5. Thus, the analytical solutions only have a unique form (a series of Case V symplectic eigenfunctions) and the trial functions could produce accurate results. However, the specific trial functions will lead to errors when the circumference wave number n for the critical buckling stress is small (e.g., a very long shell).

At last, to get a better understanding of the buckling of piezoelectric FG-NTRC cylindrical shells, the corresponding buckling modes for C-C end condition in Table 3 are presented in Figure 6. The superscript and subscript of η are the case of symplectic eigenfunctions and the circumference wave
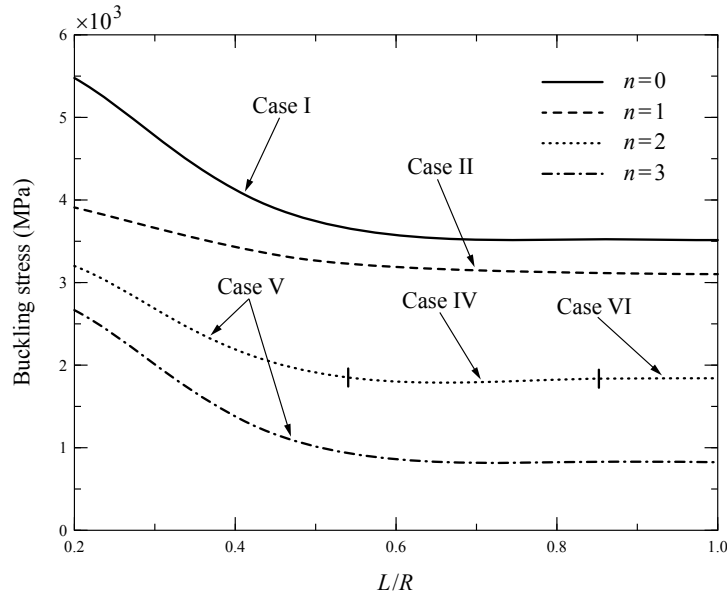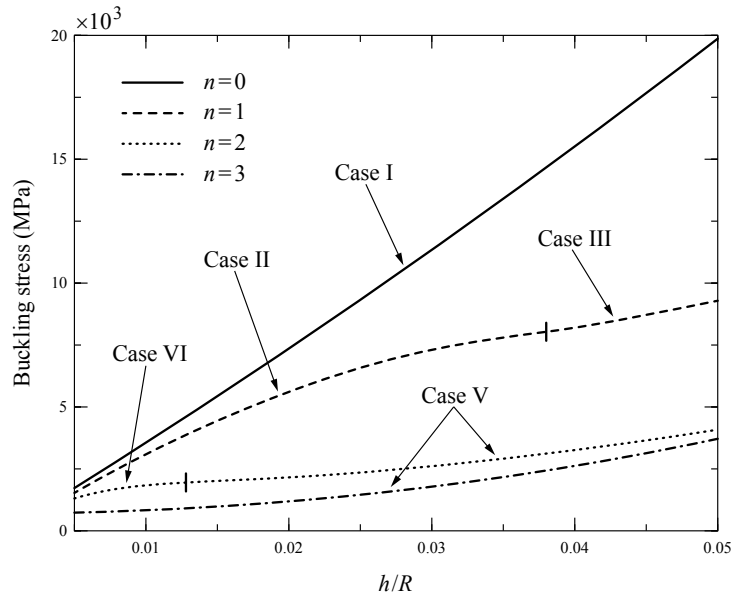
Figure 4. Variations of buckling stresses for a C-C piezoelectric FG-NTRC cylindrical shell reinforced by CNTs versus L/R with different n (FG-O, $m = 1$, $h/R = 0.01$).

number n. The color of the buckling modes is obtained by the "jet" type of the "colormap" function in Matlab. Different colors represent the displacement along the z-axes (i.e., w) of the cylindrical shell.

Figure 5. Variations of buckling stresses for a C-C piezoelectric FG-NTRC cylindrical shell reinforced by CNTs versus h/R with different n (FG-O, $m = 1$, $L/R = 1$).

n	Eigensolution	Characteristic roots					σ_{mn} (MPa)
		$L/R = 0.2$					
0	Case I	47.6496i	17.1589i	347.781	0	0	5485.46
1	Case II	37.9546i	15.2396i	0.165142i	347.783	0	3910.95
2	Case V	34.4650i	0.134607i	0.501912	19.2416	347.787	3215.40
3	Case V	32.2400i	0.400829i	0.561991	37.0153	347.794	2670.11
		$L/R = 0.5$					
0	Case I	35.1184i	23.2816i	347.781	0	0	3738.83
1	Case II	31.5626i	19.6989i	0.141165i	347.783	0	3272.59
2	Case V	16.5167i	0.188339i	2.18946	6.57829	347.787	1904.45
3	Case V	12.9775i	0.894441i	0.655560	35.3272	347.794	1014.58
		$L/R = 0.8$					
0	Case I	32.6248i	25.0611i	347.781	0	0	3555.36
1	Case II	29.1444i	21.6580i	0.136094i	347.783	0	3127.07
2	Case IV	12.8346i	0.193061i	347.787	0.752660 ± 4.18510i		1846.69
3	Case V	8.44500i	1.31099i	0.693229	35.0258	347.794	848.51
		$L/R = 1$					
0	Case I	31.8519i	25.6692i	347.781	0	0	3513.36
1	Case II	28.4520i	22.2538i	0.135052i	347.783	0	3096.72
2	Case VI	12.3684i	5.79333i	3.23354i	0.193372i	347.787	1843.09
3	Case V	7.25032i	1.50749i	0.703436	34.9646	347.794	817.80

Table 4. Buckling stresses, cases of symplectic eigenfunctions and characteristic roots for a C-C piezoelectric FG-NTRC cylindrical shell reinforced by CNTs with different L/R (FG-O, $m = 1$, $h/R = 0.01$).

$\boldsymbol{\eta}_0^{(1)}$ $(n = 0)$ $\boldsymbol{\eta}_1^{(2)}$ $(n = 1)$ $\boldsymbol{\eta}_2^{(6)}$ $(n = 2)$ $\boldsymbol{\eta}_5^{(5)}$ $(n = 5)$ $\boldsymbol{\eta}_{10}^{(5)}$ $(n = 10)$
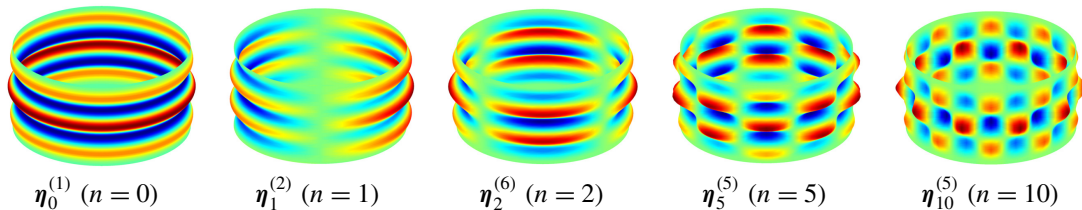
Figure 6. Buckling mode shapes for C-C piezoelectric FG-NTRC cylindrical shells with different n ($m = 1$, $L/R = 1$, $h/R = 0.01$).

6.3. *Effects of the distribution patterns of NTs, electric voltage and temperature rise.* To study the effects of the distribution patterns of NTs, electric voltage and temperature rise on the critical buckling stresses, a C-C piezoelectric NTRC cylindrical shell with $R = 0.1$ m, $L/R = 1$ and $h/R = 0.01$ is considered here. Variations of critical buckling stresses versus the volume fraction V_{NT} for different

reinforcement NTs and distribution patterns of NTs are plotted in Figure 7 with $\phi_0 = 10000\,\text{V}$ and $\Delta T = 10\,\text{K}$. It is apparent that the critical buckling stress monotonically increases with the increasing V_{NT}^* regardless of the reinforcement NTs and their distribution patterns; the critical buckling stresses for the shell reinforced by CNTs are always larger than those reinforced by BNNTs. In addition, it is also worth to note that the FG distributions produce larger critical buckling stresses than the UD when V_{NT}^* is larger than a certain value. The observation implies the FG distributions of reinforcement NTs could improve the antibuckling performance of the piezoelectric FG-NTRC cylindrical shell. The corresponding critical buckling mode shapes for $V_{NT}^* = 0.4$ in Figure 7 are presented in Figure 8. It is clear that the critical buckling mode shapes for different reinforcement NTs and distribution patterns of NTs may have different n.

The critical buckling stresses for different applied electric voltages and temperature rises are tabulated in tables 8 and 9, respectively. The computation parameters are taken as $R = 0.1\,\text{m}$, $L/R = 1$, $h/R = 0.01$, $N_{NT}^* = 0.2$, $\Delta T = 10\,\text{K}$ for Table 8 and $\phi_0 = 10000\,\text{V}$ for Table 9. It is observed that, for a specific

n	Eigensolution	Characteristic roots					σ_{mn} (MPa)
		$h/R = 0.005$					
0	Case I	47.1921i	34.6504i	695.562	0	0	1707.06
1	Case II	41.3313i	35.1534i	0.0853643i	695.563	0	1539.29
2	Case VI	36.5806i	24.0368i	0.483566i	0.105374i	695.565	1270.04
3	Case V	14.5791i	0.436957i	3.41190	12.3680	695.569	735.64
		$h/R = 0.01$					
0	Case I	31.8519i	25.6692i	347.781	0	0	3513.36
1	Case II	28.4520i	22.2538i	0.135052i	347.783	0	3096.72
2	Case VI	12.3684i	5.79333i	3.23354i	0.193372i	347.787	1843.09
3	Case V	7.25032i	1.50749i	0.703436	34.9646	347.794	817.80
		$h/R = 0.02$					
0	Case I	23.4341i	17.4449i	173.891	0	0	7363.67
1	Case II	18.1864i	12.1161i	0.258297i	173.893	0	5633.51
2	Case V	6.57791i	0.506629i	0.600103	22.4029	173.902	2135.58
3	Case V	7.07369i	1.83233i	0.531687	39.0081	173.916	1179.39
		$h/R = 0.05$					
0	Case I	16.1556i	10.1217i	69.5562	0	0	19912.16
1	Case III	7.76176i	0.451008	8.29977	69.5634	0	9295.67
2	Case V	6.41198i	0.751327i	0.355160	26.1836	69.5850	4087.02
3	Case V	7.03125i	1.90352i	0.501247	40.0669	69.6209	3708.66

Table 5. Buckling stresses, cases of symplectic eigenfunctions and characteristic roots for a C-C piezoelectric FG-NTRC cylindrical shell reinforced by CNTs with different h/R (FG-O, $m = 1$, $L/R = 1$).

n	Eigensolution	Characteristic roots					σ_{mn} (MPa)
		CNT					
0	Case I	30.1287i	24.0535i	283.790	0	0	3996.50
1	Case II	26.4194i	20.4406i	0.147932i	283.791	0	3461.30
2	Case V	8.56357i	0.527150i	2.01878	7.46659	283.797	1882.29
3	Case V	8.25457i	2.48970i	0.548627	36.2180	283.805	898.03
		BNNT					
0	Case I	23.0869i	17.0869i	284.368	0	0	2246.17
1	Case II	21.2855i	16.0233i	0.0974117i	284.370	0	1930.55
2	Case VI	16.8124i	10.5598i	0.533340i	0.211343i	284.375	1496.09
3	Case V	7.78340i	1.46291i	0.812484	12.9785	284.384	839.19

Table 6. Buckling stresses, cases of symplectic eigenfunctions and characteristic roots for a C-C piezoelectric FG-NTRC cylindrical shell with different reinforcement nanotubes (FG-X, $m = 1$, $L/R = 1$, $h/R = 0.01$).

reinforcement NT and distribution pattern, the critical buckling stress show a decreasing trend with the increase of electric voltage or temperature rise. Furthermore, it is also noted from the tabular data that the piezoelectric FG-NTRC cylindrical shell is insensitive to the electric voltage. For example, a 50×10^4 V electric voltage only leads to a 2.29% decrease of the critical buckling stress for the shell reinforced by CNT with FG-X distribution. In contrast, the piezoelectric NTRC cylindrical shell is very sensitive to the temperature rise. The critical buckling stresses significantly decreased by the temperature rise.
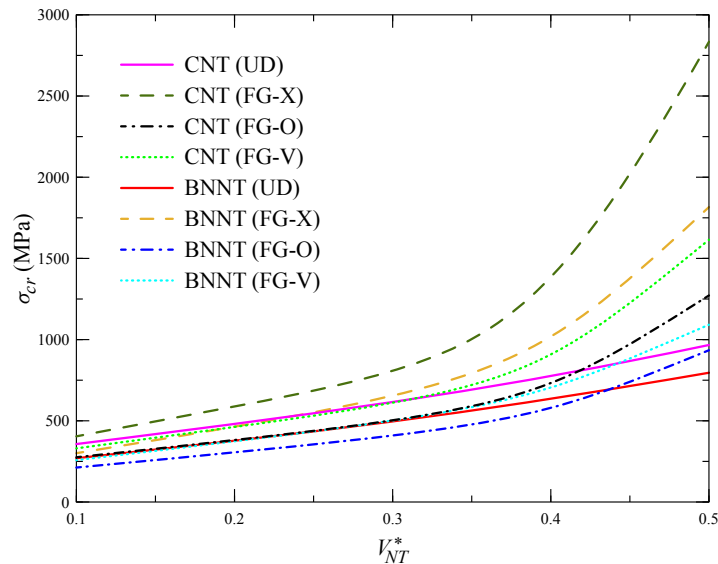
Figure 7. Critical buckling stresses (MPa) for C-C piezoelectric NTRC cylindrical shells with different V_{NT}^*.

n	Eigensolution	Characteristic roots					σ_{mn} (MPa)
		UD					
0	Case I	31.1433i	24.9141i	314.160	0	0	3718.79
1	Case II	27.4362i	21.4132i	0.142458i	314.162	0	3239.61
2	Case IV	9.43700i	0.334121i	314.167	$3.37294 \pm 2.77948i$		1823.08
3	Case V	7.86433i	2.20178i	0.577299	36.1523	314.175	837.58
		FG-X					
0	Case I	30.1287i	24.0535i	283.790	0	0	3996.50
1	Case II	26.4194i	20.4406i	0.147932i	283.791	0	3461.30
2	Case V	8.56357i	0.527150i	2.01878	7.46659	283.797	1882.29
3	Case V	8.25457i	2.48970i	0.548627	36.2180	283.805	898.30
		FG-O					
0	Case I	31.8519i	25.6692i	347.781	0	0	3513.36
1	Case II	28.4520i	22.2538i	0.135052i	347.783	0	3096.72
2	Case VI	12.3684i	5.79333i	3.23354i	0.193372i	347.787	1843.09
3	Case V	7.25032i	1.50749i	0.703436	34.9646	347.794	817.80
		FG-V					
0	Case I	31.0240i	24.8178i	314.160	0	0	3780.42
1	Case II	27.3637i	21.3602i	0.142141i	314.162	0	3300.07
2	Case IV	9.36739i	0.232799i	314.167	$3.17671 \pm 3.49833i$		1876.80
3	Case V	7.36768i	1.73605i	0.639055	35.7441	314.175	856.94

Table 7. Buckling stresses, cases of symplectic eigenfunctions and characteristic roots for a C-C piezoelectric FG-NTRC cylindrical shell reinforced by CNTs with different distribution patterns ($m = 1$, $L/R = 1$, $h/R = 0.01$).

7. Conclusion

The electro-thermo-mechanical buckling of a piezoelectric FG-NTRC cylindrical shell is investigated under the framework of Hamiltonian system. Exact solutions for buckling of piezoelectric FG-NTRC cylindrical shells are obtained and expressed in a series of symplectic eigenfunctions. Highly accurate buckling loads and analytical buckling shape functions are achieved simultaneously. The major conclusions are summarized as follows:

(1) Exact solutions for buckling of piezoelectric FG-NTRC cylindrical shells have five possible forms, which highly depend on the geometrical parameters (L/R and h/R), circumference wave numbers, reinforcement nanotubes and their distribution patterns.

(2) The influences of geometrical parameters (L/R and h/R), reinforcement NTs and their distribution patterns on expressions of symplectic eigenfunctions only occur when the circumference wave number n is small. Otherwise, the symplectic eigenfunctions only have a unique form (Case V).

Distribution	ϕ_0 (10^4 V)				
	-50	-25	0	25	50
	CNT				
UD	488.913	482.232	475.550	468.868	462.187
FG-X	595.554	588.879	582.204	575.529	568.854
FG-O	389.925	383.250	376.575	369.900	363.225
FG-V	473.930	467.255	460.580	453.905	447.230
	BNNT				
UD	383.596	378.388	373.181	367.974	362.766
FG-X	463.227	458.158	453.088	448.018	442.949
FG-O	311.640	306.571	301.501	296.431	291.362
FG-V	350.880	345.811	340.741	335.671	330.602

Table 8. Critical buckling stresses (MPa) for a C-C piezoelectric NTRC cylindrical shell with different electric voltage ϕ_0.

CNT, UD ($n = 5$)   CNT, FG-X ($n = 5$)   CNT, FG-O ($n = 6$)   CNT, FG-V ($n = 6$)

BNNT, UD ($n = 6$)   BNNT, FG-X ($n = 5$)   BNNT, FG-O ($n = 7$)   BNNT, FG-V ($n = 6$)
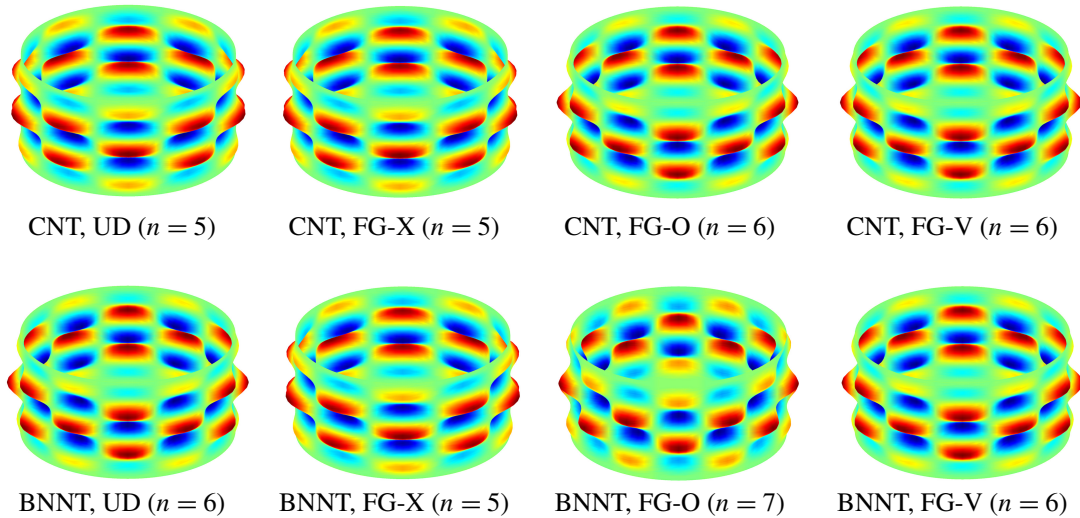
Figure 8. Critical buckling mode shapes for C-C piezoelectric NTRC cylindrical shells with different reinforcement NTs and distribution patterns ($L/R = 1$, $h/R = 0.01$).

(3) The FG distribution of NTs could increase the carrying capacity of piezoelectric FG-NTRC cylindrical shells compared to uniform piezoelectric NTRC cylindrical shells. The FG-X shell produces the highest critical buckling stress.

(4) The applied electric voltages and temperature rises could affect the carrying capacity of piezoelectric FG-NTRC cylindrical shells. The critical buckling stresses are sensitive to the temperature rise but insensitive to the electric voltage.

Distribution	ΔT				
	0	5	10	15	20
CNT					
UD	663.957	569.620	475.283	380.946	286.609
FG-X	770.611	676.274	581.937	487.600	393.263
FG-O	564.982	470.645	376.308	281.971	187.634
FG-V	648.987	554.650	460.313	365.976	271.639
BNNT					
UD	516.471	444.722	372.973	301.224	229.475
FG-X	596.383	524.634	452.885	381.136	309.387
FG-O	444.796	373.047	301.298	229.549	157.800
FG-V	484.036	412.287	340.538	268.789	197.040

Table 9. Critical buckling stresses (MPa) for a C-C piezoelectric NTRC cylindrical shell with different temperature rise ΔT.

Appendix A

$$H = \begin{bmatrix} H_1 & H_2 \\ H_3 & -H_1^{\mathrm{T}} \end{bmatrix}, \tag{A.1}$$

$$H_1 = \begin{bmatrix} 0 & \left(\frac{B_{66}}{A_{66}} - R\right)\frac{\partial}{\partial x} & 0 & -2\frac{RB_{66}}{A_{66}}\frac{\partial}{\partial x} & 0 \\ \frac{R\kappa_3}{\kappa_2}\frac{\partial}{\partial x} & 0 & \frac{R\kappa_5}{\kappa_2}\frac{\partial^2}{\partial x^2} - 1 & 0 & \frac{RB_{22}E_{32}}{\kappa_2} \\ 0 & 1 & 0 & -R & 0 \\ -R\frac{\kappa_4}{\kappa_2}\frac{\partial}{\partial x} & 0 & R\frac{\kappa_6}{\kappa_2}\frac{\partial^2}{\partial x^2} & 0 & -\frac{RA_{22}E_{32}}{\kappa_2} \\ 0 & 0 & 0 & 0 & 0 \end{bmatrix}, \tag{A.2}$$

$$H_2 = \begin{bmatrix} \frac{R}{A_{66}} & 0 & 0 & 0 & 0 \\ 0 & \frac{RD_{22}}{\kappa_2} & 0 & -\frac{RB_{22}}{\kappa_2} & 0 \\ 0 & 0 & 0 & 0 & 0 \\ 0 & -\frac{RB_{22}}{\kappa_2} & 0 & \frac{RA_{22}}{\kappa_2} & 0 \\ 0 & 0 & 0 & 0 & -\frac{1}{RX_{22}} \end{bmatrix}, \tag{A.3}$$

$$H_3 = \begin{bmatrix} \frac{R\kappa_{10}}{D_{22}\kappa_2}\frac{\partial^2}{\partial x^2} & 0 & \frac{R\kappa_{11}}{D_{22}\kappa_2}\frac{\partial^3}{\partial x^3} & 0 & RE_{32}\frac{\kappa_4}{\kappa_2}\frac{\partial}{\partial x} \\ 0 & -\frac{\kappa_9}{R}\frac{\partial^2}{\partial x^2} & 0 & 2\kappa_9\frac{\partial^2}{\partial x^2} & 0 \\ -\frac{R\kappa_{11}}{D_{22}\kappa_2}\frac{\partial^3}{\partial x^3} & 0 & -\frac{R\kappa_{12}}{D_{22}\kappa_2}\frac{\partial^4}{\partial x^4} + RN_x^0\frac{\partial^2}{\partial x^2} & 0 & -R\left(E_{31} - \frac{\kappa_6}{\kappa_2}E_{32}\right)\frac{\partial^2}{\partial x^2} \\ 0 & 2\kappa_9\frac{\partial^2}{\partial x^2} & 0 & -4R\kappa_9\frac{\partial^2}{\partial x^2} & 0 \\ -RE_{32}\frac{\kappa_4}{\kappa_2}\frac{\partial}{\partial x} & 0 & -R\left(E_{31} - \frac{\kappa_6}{\kappa_2}E_{32}\right)\frac{\partial^2}{\partial x^2} & 0 & R\left(X_{11}\frac{\partial^2}{\partial x^2} - X_{33} - \frac{A_{22}E_{32}^2}{\kappa_2}\right) \end{bmatrix}. \tag{A.4}$$

Appendix B

$$\xi_1^{(0)} = \frac{A_{11}E_{31}^2 R + (2A_{11}B_{12} - 2A_{12}B_{11} - A_{11}N_x^0 R)X_{11} + (A_{11}D_{11} - B_{11}^2)RX_{33}}{(B_{11}^2 - A_{11}D_{11})RX_{11}} \tag{B.1}$$

$$\xi_2^{(0)} = \frac{(A_{12}^2 - A_{11}A_{22})X_{11} + R(2A_{12}B_{11} - 2A_{11}B_{12} + A_{11}N_x^0 R)X_{33}}{(B_{11}^2 - A_{11}D_{11})R^2 X_{11}}, \tag{B.2}$$

$$\xi_3^{(0)} = \frac{(-A_{12}^2 + A_{11}A_{22})X_{33}}{(B_{11}^2 - A_{11}D_{11})R^2 X_{11}}, \tag{B.3}$$

$$\xi_4^{(0)} = 0 \quad \text{and} \quad \xi_5^{(0)} = 0. \tag{B.4}$$

Appendix C

$$
\begin{aligned}
\xi_1 = {}& \frac{1}{(B_{11}^2 - A_{11}D_{11})R^6(D_{66} + 2B_{66}R + A_{66}R^2)X_{11}} \\
& \times \Big\{ -\big(B_{66}^2 D_{11} - 2B_{11}B_{66}D_{12} + B_{11}^2 D_{22} - A_{66}D_{11}D_{66}\big)n^2 X_{11} \\
& \quad - 2A_{12}B_{11}D_{66}RX_{11} - 2\big(B_{11}^2 B_{22} + A_{12}B_{66}D_{11}\big)n^2 RX_{11} \\
& \quad - 2B_{11}\big[2B_{66}^2 - (A_{12} + A_{66})(D_{12} + 2D_{66})\big]n^2 RX_{11} - 4A_{12}B_{11}B_{66}R^2 X_{11} \\
& \quad - [B_{11}(A_{22}B_{11} - 4A_{12}B_{66}) + A_{12}(A_{12} + 2A_{66})D_{11}]n^2 R^2 X_{11} \\
& \quad - 2A_{12}A_{66}B_{11}R^3 X_{11} - B_{12}^2 n^2(D_{11} - 2B_{11}R)X_{11} \\
& \quad + 2B_{12}n^2[-(A_{12} + A_{66})D_{11}R + B_{66}(-D_{11} + B_{11}R) + B_{11}(D_{12} + D_{66} + A_{12}R^2)]X_{11} \\
& \quad - B_{11}^2 D_{66}n^2 R^2 X_{22} - 2B_{11}^2 B_{66}n^2 R^3 X_{22} - A_{66}B_{11}^2 n^2 R^4 X_{22} \\
& \quad - B_{11}^2 R^2[D_{66} + R(2B_{66} + A_{66}R)]X_{33} + A_{11}(-D_{12}^2 + D_{12}D_{22})n^2 X_{11} \\
& \quad + A_{11}D_{66}\big[-2D_{12}n^2 X_{11} + 2B_{12}(1 - 2n^2)RX_{11} \\
& \qquad\qquad\qquad\quad + R^2\big(E_{31}^2 + 4A_{66}n^2 X_{11} - N_x^0 X_{11} + D_{11}n^2 X_{22} + D_{11}X_{33}\big)\big] \\
& \quad + A_{11}R\big[-4B_{66}^2 n^2 RX_{11} + n^2\big(2B_{22}D_{11} - 2B_{12}D_{12} - B_{12}^2 R + A_{22}D_{11}R\big)X_{11} \\
& \qquad\quad - 4B_{12}B_{66}R(-1 + n^2)X_{11} + 2B_{66}R^2\big(E_{31}^2 - N_x^0 X_{11} + D_{11}n^2 X_{22} + D_{11}X_{33}\big) \\
& \qquad\quad + A_{66}R\big(2D_{12}n^2 X_{11} + 2B_{12}RX_{11}\big) \\
& \qquad\qquad\qquad\qquad\quad + A_{66}R^3\big(E_{31}^2 - N_x^0 X_{11} + D_{11}n^2 X_{22} + D_{11}X_{33}\big)\big]\Big\}, \quad (C.1)
\end{aligned}
$$

$$
\begin{aligned}
\xi_2 = {}& \frac{1}{(B_{11}^2 - A_{11}D_{11})R^4(D_{66} + 2B_{66}R + A_{66}R^2)X_{11}} \\
& \times \big\{ -2B_{12}^2 n^2(-1 + n^2)RX_{11}
\end{aligned}
$$

$$- 2A_{12}B_{11}n^2R\big[E_{31}E_{32}R^2 + (-1+n^2)(D_{22}+B_{22}R)X_{11}$$
$$- D_{66}R^2X_{22} + (D_{12}+2D_{66})n^2R^2X_{22}\big]$$
$$+ B_{11}^2n^2R\big[E_{32}^2 + n^2\big(D_{22}+2B_{22}R+A_{22}R^2\big)X_{22}\big] + A_{12}^2D_{66}R^2X_{11}$$
$$+ A_{12}^2n^2R^2\big[2(D_{12}+2D_{66})(-1+n^2)X_{11} + R^2\big(E_{31}^2 - N_x^0X_{11} + D_{11}n^2X_{22}\big)\big]$$
$$+ A_{66}2A_{12}E_{31}^2n^2R^4$$
$$+ A_{66}\big(D_{12}^2n^4 - D_{11}D_{22}n^4 - 2B_{22}D_{11}n^4R - 2A_{12}D_{12}n^2R^2 - A_{22}D_{11}n^4R^2$$
$$+ 4A_{12}D_{12}n^4R^2 + A_{12}^2R^2 - 2A_{12}n^2N_x^0R^4\big)X_{11}$$
$$+ 2A_{12}A_{66}D_{11}n^4R^4X_{22} - 2A_{66}D_{12}D_{66}n^4X_{11}$$
$$+ A_{66}D_{66}n^2R^2\big[E_{31}^2 - \big(-4A_{12}+8A_{12}n^2+N_x^0\big)X_{11} + n^2(D_{11}+4B_{11}R)X_{22}\big]$$
$$+ 2A_{66}B_{11}n^2R\big[D_{22}n^2X_{11} + B_{22}(1+n^2)RX_{11}$$
$$+ R^2\big(E_{31}E_{32} + A_{22}X_{11} + D_{12}n^2X_{22} - A_{12}R^2X_{22}\big)\big]$$
$$- A_{11}D_{22}n^2R^2\big[\big(E_{31}^2 + A_{66}n^2X_{11} - N_x^0X_{11} + D_{11}n^2X_{22}\big) + D_{66}n^2X_{11}\big]$$
$$+ A_{11}D_{12}^2n^4R^2X_{22} + 2A_{11}D_{66}E_{31}E_{32}n^2R^2$$
$$- A_{11}D_{66}R(-1+2n^2)[-A_{22}R + 2n^2(B_{22}+A_{22}R)]X_{11}$$
$$- A_{11}D_{66}n^2R^4X_{22}\big(4A_{66}n^2 - N_x^0\big)$$
$$- 2A_{11}D_{12}n^2R[-E_{31}E_{32}R + (-1+n^2)(B_{22}+A_{22}R)X_{11}$$
$$+ n^2R\big(-D_{66}+A_{66}R^2\big)X_{22}]$$
$$- A_{11}D_{11}n^4R^3(2B_{22}+A_{22}R)X_{22} - A_{11}D_{11}n^2R^2E_{32}^2$$
$$- 2A_{11}R^3B_{22}n^2\big[E_{31}^2 + \big(A_{66}-N_x^0\big)X_{11}\big]$$
$$- A_{11}R^4\big[A_{22}\big(A_{66}X_{11} + E_{31}^2n^2 - N_x^0n^2X_{11}\big) + A_{66}n^2\big(2E_{31}E_{32} - N_x^0R^2X_{22}\big)\big]$$
$$+ R^2\big[B_{11}^2D_{22} - A_{66}D_{11}D_{66} + A_{11}\big(D_{12}^2 - D_{11}D_{22} + 2D_{12}D_{66}\big)\big]n^2X_{33}$$
$$- 2\big[-B_{11}^2B_{22} + A_{11}B_{22}D_{11} + (A_{12}+A_{66})B_{11}(D_{12}+2D_{66})\big]n^2R^3X_{33}$$
$$+ 2A_{12}B_{11}D_{66}R^3X_{33} + \big[A_{12}^2D_{11} + 2A_{12}A_{66}D_{11} + A_{22}\big(B_{11}^2 - A_{11}D_{11}\big)$$
$$- 2A_{11}A_{66}(D_{12}+2D_{66})\big]n^2R^4X_{33}$$
$$+ A_{11}D_{66}N_x^0R^4X_{33} + R^2\big(2A_{12}A_{66}B_{11}R^3 + A_{11}A_{66}N_x^0R^4\big)X_{33} - 2B_{66}^2D_{12}n^4X_{11}$$
$$+ B_{66}^2n^2\big[E_{31}^2R^2 + 4A_{12}(1-2n^2)R^2X_{11} - N_x^0R^2X_{11}$$
$$+ R^2\big(D_{11}+4B_{11}R+4A_{11}R^2\big)\big(n^2X_{22}+X_{33}\big)\big]$$
$$+ B_{12}^2n^2\big[D_{66}n^2X_{11} + 4B_{66}(1-2n^2)RX_{11} + E_{31}^2R^2 + 4A_{66}R^2X_{11}$$
$$- 2A_{12}(-1+n^2)R^2X_{11} - N_x^0R^2X_{11}$$
$$+ R^2\big(D_{11}-2B_{11}R+A_{11}R^2\big)\big(n^2X_{22}+X_{33}\big)\big]$$
$$- 2B_{12}B_{66}^2n^2(-1+4n^2)RX_{11} - 2B_{12}B_{66}D_{12}n^4X_{11}$$

$$+ 2B_{12}B_{66}n^2R^2\big[(A_{12} - 4A_{12}n^2 - N_x^0)X_{11} + E_{31}^2$$
$$+ (D_{11}n^2 - B_{11}n^2R - 2A_{11}R^2 + 2A_{11}n^2R^2)X_{22}\big]$$
$$- 2B_{12}B_{66}R^2\big[-D_{11}n^2 + 2A_{11}R^2 + n^2R(B_{11} - 2A_{11}R)\big]X_{33}$$
$$- 2A_{11}B_{12}n^2R\big[-E_{31}E_{32}R^2 - (-1 + n^2)(D_{22} + B_{22}R)X_{11}$$
$$+ (D_{66} - D_{12}n^2 + 2D_{66}n^2)R^2X_{22}\big]$$
$$- 2A_{66}B_{12}n^2R\big[(D_{66} - 2D_{12}n^2 + 2D_{66}n^2)X_{11}$$
$$+ R^2(-E_{31}^2 + N_x^0X_{11} - D_{11}n^2X_{22} + A_{11}R^2X_{22})\big]$$
$$- 2B_{12}R^3\big[-A_{66}D_{11}n^2 + A_{11}(D_{66} - D_{12}n^2 - 2D_{66}n^2 + A_{66}R^2)\big]X_{33}$$
$$+ 2A_{12}B_{12}n^2R\big[(-D_{12} - D_{66} + D_{12}n^2 + 2D_{66}n^2)X_{11}$$
$$+ R^2(E_{31}^2 + 2A_{66}X_{11} - N_x^0X_{11} + D_{11}n^2X_{22} + D_{11}X_{33})\big]$$
$$+ 2B_{11}B_{12}B_{22}(-1 + n^2)n^2RX_{11}$$
$$- 2B_{11}B_{12}n^2R^2\big[E_{31}E_{32} + A_{22}(1 - n^2)X_{11} + (D_{12} + B_{66} + A_{12}R^2)(n^2X_{22} + X_{33})\big]$$
$$+ 2B_{66}(A_{12}^2 - A_{11}A_{22})R^3X_{11}$$
$$+ 2B_{66}n^4\big[A_{11}R(D_{22} + 2B_{22}R)X_{11} + B_{11}(D_{22} + 3B_{22}R + 2A_{22}R^2)X_{11}$$
$$+ A_{12}D_{11}R^3X_{22} - B_{11}R^2(D_{12} + 2A_{12}R^2)X_{22}\big]$$
$$+ 4A_{12}B_{11}B_{66}R^4X_{33} + 2A_{11}B_{66}N_x^0R^5X_{33} - 4A_{12}^2B_{66}n^2R^3X_{11}$$
$$+ 2A_{11}B_{66}n^2R^3(2A_{22}X_{11} + N_x^0R^2X_{22})$$
$$- 2A_{12}B_{66}n^2R\big[D_{12}X_{11} - R^2(E_{31}^2 - N_x^0X_{11} + D_{11}X_{33})\big]$$
$$- 2B_{11}B_{66}n^2R[B_{22}X_{11} + E_{31}E_{32}R + A_{22}RX_{11}$$
$$+ D_{12}RX_{33} + 2A_{12}R^3(-X_{22} + X_{33})]\big\}, \quad \text{(C.2)}$$

$$\xi_3 = \frac{1}{(B_{11}^2 - A_{11}D_{11})R^6(D_{66} + 2B_{66}R + A_{66}R^2)X_{11}}$$
$$\times \big\{2B_{66}^2E_{31}E_{32}n^4R^2 - B_{66}^2n^2[D_{22}n^4 + (1 - 2n)^2R(A_{22}R - 2B_{22}n^2 - 2A_{22}n^2R)]X_{11}$$
$$- B_{66}^2n^4R^2\big[2D_{12}n^2 - (4A_{12} - 8A_{12}n^2 - N_x^0)R^2\big]X_{22} - 2A_{12}^2B_{66}n^2(1 - 2n^2)R^5X_{22}$$
$$- 2A_{11}B_{66}n^2R^3\big[E_{32}^2n^2 + D_{22}n^4X_{22} + 2B_{22}n^4RX_{22} + A_{22}(-1 + 2n^2)R^2X_{22}\big]$$
$$- 2B_{11}B_{66}E_{32}^2n^4R^2 - 2B_{11}B_{66}n^4R^2\big[D_{22}n^2 + B_{22}(-1 + 3n^2)R + A_{22}(-1 + 2n^2)R^2\big]X_{22}$$
$$+ 2A_{12}B_{66}n^2R\big[E_{31}E_{32}R^2 + (-1 + n^2)(-B_{22}R + D_{22}n^2 + 2B_{22}n^2R)X_{11}$$
$$+ n^2R^2(D_{12} + N_x^0R^2)X_{22}\big]$$
$$- A_{12}(-1 + n^2)n^2R^2\big[2E_{32}R(-B_{11}E_{32} + A_{12}E_{31}R) + A_{12}D_{22}(-1 + n^2)X_{11}\big]$$

$$- A_{12}^2 D_{66} n^2 R^4 X_{22} - A_{12} n^4 R^3 [2A_{12}(D_{12} + 2D_{66})(-1 + n^2)R$$
$$- A_{12} N_x^0 R^3 - 2B_{11}(-1 + n^2)(D_{22} + B_{22}R)]X_{22}$$
$$- A_{11} n^2 R^2 \big[-D_{66} E_{32}^2 n^2 - A_{22} D_{22}(1 - n^2)X_{11} + 2A_{22} E_{31} E_{32}(1 - n^2)R^2$$
$$+ E_{32}^2 N_x^0 R^2 - A_{22} D_{22} n^4 X_{11} + B_{22}^2 (1 - n^2)^2 X_{11}$$
$$+ n^2 R^2 \big(2A_{22} D_{12} - 2A_{22} D_{12} n^2 + D_{22} N_x^0 + A_{22} N_x^0 R^2 \big) X_{22} \big]$$
$$+ A_{11} D_{66} n^2 R^2 [D_{22} n^4 + (-1 + 2n^2)R(-A_{22}R + 2B_{22}n^2 + 2A_{22}n^2 R)]X_{22}$$
$$- 2A_{11} B_{22} n^2 R^3 \big[E_{31} E_{32}(1 - n^2) + n^2 \big(D_{12} - D_{12} n^2 + N_x^0 R^2 \big) X_{22} \big]$$
$$+ B_{66}^2 n^2 R^2 \big[2D_{12} n^2 + A_{12}(-4 + 8n^2)R^2 + N_x^0 R^2 \big] X_{33} - 2B_{11} B_{66} D_{22} n^4 R^2 X_{33}$$
$$+ 2B_{66} [B_{11} B_{22} + A_{12} D_{12} - (3B_{11} B_{22} + A_{11} D_{22})n^2] n^2 R^3 X_{33}$$
$$+ 2B_{66} [A_{22} B_{11} - 2(A_{22} B_{11} + A_{11} B_{22})n^2] n^2 R^4 X_{33}$$
$$+ 2B_{66} \big[\big(A_{12}^2 - A_{11} A_{22} \big)(-1 + 2n^2) + A_{12} n^2 N_x^0 \big] R^5 X_{33} - A_{12}^2 D_{66} R^4 X_{33}$$
$$- A_{12}^2 D_{66} R^4 X_{33} + A_{12} \big[-2A_{12}(D_{12} + 2D_{66})(-1 + n^2)R + A_{12} N_x^0 R^3$$
$$+ 2B_{11}(-1 + n^2)(D_{22} + B_{22}R) \big] n^2 R^3 X_{33}$$
$$+ A_{11} D_{22} \big(D_{66} n^4 - n^2 N_x^0 R^2 \big) R^2 X_{33}$$
$$+ 2A_{11} B_{22} \big[-D_{12} - D_{66} + (D_{12} + 2D_{66})n^2 - N_x^0 R^2 \big] n^2 R^3 X_{33}$$
$$+ A_{11} A_{22} \big[D_{66}(1 - 2n^2)^2 + 2D_{12}(-1 + n^2)n^2 - N_x^0 n^2 R^2 \big] R^4 X_{33}$$
$$+ 2B_{12}^3 n^2 (-1 + n^2)R^3 (n^2 X_{22} + X_{33})$$
$$+ B_{12}^2 n^2 R^2 \big[-\big(D_{66} n^2 + 4B_{66}R - 8B_{66} n^2 R + 2A_{12} R^2$$
$$- 2A_{12} n^2 R^2 - N_x^0 R^2 \big)(n^2 X_{22} + X_{33}) - A_{22}(-1 + n^2)^2 X_{11} \big]$$
$$+ 2B_{12} B_{66}^2 n^2 (-1 + 4n^2)R^3 (n^2 X_{22} + X_{33})$$
$$+ 2B_{12} B_{66} n^2 R \big[-B_{12} n^2 (-1 + n^2)X_{11} + A_{22}(-1 + 3n^2 - 2n^4)RX_{11} + E_{31} E_{32} n^2 R$$
$$+ \big(D_{12} n^2 R - A_{12} R^3 + 4A_{12} n^2 R^3 + N_x^0 R^3 \big)(n^2 X_{22} + X_{33}) \big]$$
$$+ 2A_{11} B_{12} n^2 R^2 \big[E_{31} E_{32}(1 - n^2)R + B_{22}(1 - n^2)^2 X_{11}$$
$$+ R \big(D_{12} + D_{66} - (D_{12} + 2D_{66})n^2 + N_x^0 R^2 \big)(n^2 X_{22} + X_{33}) \big]$$
$$+ 2A_{11} B_{12} n^2 R^3 (1 - n^2)[E_{32}^2 + (D_{22} + B_{22}R)(n^2 X_{22} + X_{33})]$$
$$+ 2B_{11} B_{12} n^2 R^3 (1 - n^2)[(B_{22} + A_{22}R)(n^2 X_{22} + X_{33})]$$
$$+ A_{66} D_{22} n^4 [D_{66} n^2 X_{11} - 2B_{12}(-1 + n^2)RX_{11}]$$
$$+ A_{66} D_{22} n^4 R^2 [-2A_{12}(-1 + n^2)X_{11} + E_{31}^2 - N_x^0 X_{11}$$
$$+ (D_{11} + 2B_{11}R + A_{11}R^2)(n^2 X_{22} + X_{33})]$$
$$- 2A_{66} D_{12} n^4 R \big[E_{31} E_{32} R + (1 - n^2)(B_{22} + A_{22}R)X_{11}$$
$$+ D_{66} n^2 R - A_{12} R^3 X_{22} + 2n^2 R^2 (B_{12} + A_{12}R)X_{22} \big]$$

$$- 2A_{66}D_{12}n^2R^2[D_{66}n^2 - A_{12}R^2 + 2n^2R(B_{12} + A_{12}R)]X_{33} - A_{66}D_{12}^2n^4R^2(n^2X_{22} + X_{33})$$

$$+ A_{66}D_{66}n^2R\big[-2E_{31}E_{32}n^2R + 2B_{22}n^2(-1 + 2n^2)X_{11} + A_{22}(1 - 2n^2)^2RX_{11}$$

$$- R^2(-2B_{12} + 8B_{12}n^2 - 4A_{12}R + 8A_{12}n^2R + N_x^0R)(n^2X_{22} + X_{33})\big]$$

$$+ A_{66}D_{11}n^4R^2[E_{32}^2 + R(2B_{22} + A_{22}R)(n^2X_{22} + X_{33})]$$

$$+ A_{66}n^2R^3\big[-4B_{12}^2n^2RX_{22} + 2B_{11}n^2\big(E_{32}^2 + A_{22}R^2X_{22}\big)\big]$$

$$+ A_{66}n^2R^4\big[2A_{12}E_{31}E_{32} + A_{22}E_{31}^2n^2 - 4A_{12}E_{31}E_{32}n^2 + A_{11}E_{32}^2n^2 - A_{22}n^2N_x^0X_{11}$$

$$+ \big(-A_{12}^2 + A_{11}A_{12} + 2A_{12}n^2N_x^0\big)R^2X_{22}\big]$$

$$+ 2A_{66}B_{12}n^2R^3\big[-A_{22}X_{11} + n^2\big(-2E_{31}E_{32} + A_{22}X_{11} - 2A_{12}R^2X_{22} + N_x^0R^2X_{22}\big)\big]$$

$$+ A_{66}R^4\big[-4B_{12}^2n^2 + 2n^2\big(A_{22}B_{11} - 2A_{12}B_{12} + B_{12}N_x^0\big)R$$

$$+ \big(-A_{12}^2 + A_{11}A_{12} + 2A_{12}n^2N_x^0\big)R^2\big]X_{33}$$

$$+ 2A_{66}B_{22}n^2R^3\big[A_{12}X_{11} + E_{31}^2n^2 - \big(A_{12} + N_x^0\big)n^2X_{11}$$

$$+ n^2R(B_{11} + B_{11}n^2 + A_{11}R)X_{22} + R(B_{11} + B_{11}n^2 + A_{11}R)X_{33}\big]\Big\}, \quad \text{(C.3)}$$

$$\xi_4 = \frac{1}{\big(B_{11}^2 - A_{11}D_{11}\big)R^6(D_{66} + 2B_{66}R + A_{66}R^2)X_{11}}$$

$$\times \Big\{B_{66}^2E_{32}^2n^6 + B_{66}^2n^2(n^2X_{22} + X_{33})[D_{22}n^4 + (-1 + 2n^2)(-A_{22}R^2 + 2B_{22}n^2R + 2A_{22}n^2R^2)]$$

$$- 2B_{66}(-1 + n^2)n^2R[A_{12}E_{32}^2n^2 - B_{12}(-A_{22}R + B_{22}n^2 + 2A_{22}n^2R)(n^2X_{22} + X_{33})$$

$$+ A_{12}(-B_{22}R + D_{22}n^2 + 2B_{22}n^2R)(n^2X_{22} + X_{33})]$$

$$+ A_{66}n^4\big[-2A_{12}E_{32}^2R^2 + 2A_{12}E_{32}^2n^2R^2 + E_{32}^2N_x^0R^2 + B_{22}^2X_{11} - 2B_{22}^2n^2X_{11} + B_{22}^2n^4X_{11}$$

$$- A_{22}(-1 + n^2)(2E_{31}E_{32}R^2 - D_{22} + D_{22}n^2X_{11})$$

$$+ D_{22}n^2\big(-2A_{12} + 2A_{12}n^2 + N_x^0\big)R^2X_{22}$$

$$+ A_{22}n^2R^2\big(2D_{12} - 2D_{12}n^2 + N_x^0R^2\big)X_{22}$$

$$+ 2B_{12}(-1 + n^2)R\big(E_{32}^2 + D_{22}n^2X_{22} - A_{22}R^2X_{22}\big)\big]$$

$$+ 2A_{66}B_{12}n^2R(-1 + n^2)(D_{12}n^2 - A_{22}R^2)X_{33}$$

$$+ A_{66}n^4R^2\big[D_{22}\big(-2A_{12} + 2A_{12}n^2 + N_x^0\big) + A_{22}\big(2D_{12} - 2D_{12}n^2 + N_x^0R^2\big)\big]X_{33}$$

$$- 2A_{66}B_{22}E_{31}E_{32}n^4(-1 + n^2)R$$

$$- 2A_{66}B_{22}n^2R\big[A_{12}R^2 + D_{12}(-1 + n^2)n^2 - \big(A_{12} + N_x^0\big)n^2R^2\big](n^2X_{22} + X_{33})$$

$$- A_{66}D_{66}n^2\big[D_{22}n^4 + (-1 + 2n^2)R(-A_{22}R + 2B_{22}n^2 + 2A_{22}n^2R)\big](n^2X_{22} + X_{33})$$

$$- A_{66}D_{66}E_{32}^2n^6$$

$$+ (-1 + n^2)^2n^2R^2\big[A_{22}B_{12}^2(n^2X_{22} + X_{33}) - 2A_{12}B_{12}B_{22}(n^2X_{22} + X_{33})$$

$$+ A_{12}^2\left(E_{32}^2 + D_{22}n^2 X_{22} + D_{22}X_{33}\right) + A_{11}B_{22}^2(n^2 X_{22} + X_{33})$$
$$- A_{11}A_{22}\left(E_{32}^2 + D_{22}n^2 X_{22} + D_{22}X_{33}\right)]\Big\}, \quad \text{(C.4)}$$

$$\xi_5 = \frac{1}{\left(B_{11}^2 - A_{11}D_{11}\right)R^6(D_{66} + 2B_{66}R + A_{66}R^2)X_{11}}$$
$$\times \{A_{66}n^4(1-n^2)^2[-B_{22}^2(n^2 X_{22} + X_{33}) + A_{22}E_{32}^2 + A_{22}D_{22}(n^2 X_{22} + X_{33})]\}. \quad \text{(C.5)}$$

Acknowledgments

References

[Ansari et al. 2016] R. Ansari, T. Pourashraf, R. Gholami, and A. Shahabodini, "Analytical solution for nonlinear postbuckling of functionally graded carbon nanotube-reinforced composite shells with piezoelectric layers", *Compos. B Eng.* **90** (2016), 267–277.

[Chen and Zhao 2009] W. Q. Chen and L. Zhao, "The symplectic method for plane elasticity problem of functionally graded materials", *Acta Mech. Sinica* **41**:4 (2009), 588–594. in Chinese.

[Chen et al. 1996] C.-Q. Chen, Y.-P. Shen, and X.-M. Wang, "Exact solution of orthotropic cylindrical shell with piezoelectric layers under cylindrical bending", *Int. J. Solids Struct.* **33**:30 (1996), 4481–4494.

[Dai and Zheng 2011] H.-L. Dai and H.-Y. Zheng, "Buckling and post-buckling analyses for an axially compressed laminated cylindrical shell of FGM with PFRC in thermal environments", *Eur. J. Mech. A Solids* **30**:6 (2011), 913–923.

[Dai et al. 2013] H.-L. Dai, T. Dai, and H.-Y. Zheng, "Creep buckling and post-buckling analyses for a hybrid laminated viscoelastic FGM cylindrical shell under in-plane loading", *Int. J. Mech. Mater. Des.* **9**:4 (2013), 309–323.

[Dong and Wang 2007] K. Dong and X. Wang, "Wave propagation characteristics in piezoelectric cylindrical laminated shells under large deformation", *Compos. Struct.* **77**:2 (2007), 171–181.

[Fan and Wang 2016] Y. Fan and H. Wang, "The effects of matrix cracks on the nonlinear bending and thermal postbuckling of shear deformable laminated beams containing carbon nanotube reinforced composite layers and piezoelectric fiber reinforced composite layers", *Compos. B Eng.* **106** (2016), 28–41.

[Farajpour et al. 2017] A. Farajpour, A. Rastgoo, and M. Mohammadi, "Vibration, buckling and smart control of microtubules using piezoelectric nanoshells under electric voltage in thermal environment", *Physica B* **509** (2017), 100–114.

[Fard and Bohlooly 2017] K. M. Fard and M. Bohlooly, "Postbuckling of piezolaminated cylindrical shells with eccentrically/concentrically stiffeners surrounded by nonlinear elastic foundations", *Compos. Struct.* **171** (2017), 360–369.

[Ganesan and Kadoli 2003] N. Ganesan and R. Kadoli, "Buckling and dynamic analysis of piezothermoelastic composite cylindrical shell", *Compos. Struct.* **59**:1 (2003), 45–60.

[Ghorbanpour Arani et al. 2012a] A. Ghorbanpour Arani, S. Amir, A. R. Shajari, and M. R. Mozdianfard, "Electro-thermo-mechanical buckling of DWBNNTs embedded in bundle of CNTs using nonlocal piezoelasticity cylindrical shell theory", *Compos. B Eng.* **43**:2 (2012), 195–203.

[Ghorbanpour Arani et al. 2012b] A. Ghorbanpour Arani, S. Shams, S. Amir, and M. J. Maboudi, "Buckling of piezoelectric composite cylindrical shell under electro-thermo-mechanical loading", *J. Solid Mech.* **4**:3 (2012), 296–306.

[Ghorbanpour Arani et al. 2014] A. Ghorbanpour Arani, A. A. M. Barzoki, and R. Kolahchi, "Nonlinear dynamic buckling of viscous-fluid-conveying PNC cylindrical shells with core resting on visco-Pasternak medium", *J. Solid Mech.* **6**:3 (2014), 265–277.

[Ghorbanpour Arani et al. 2016] A. Ghorbanpour Arani, M. Jamali, M. Mosayyebi, and R. Kolahchi, "Wave propagation in FG-CNT-reinforced piezoelectric composite micro plates using viscoelastic quasi-3D sinusoidal shear deformation theory", *Compos. B Eng.* **95** (2016), 209–224.

[Hajmohammad et al. 2017] M. H. Hajmohammad, M. S. Zarei, A. Nouri, and R. Kolahchi, "Dynamic buckling of sensor/functionally graded-carbon nanotube-reinforced laminated plates/actuator based on sinusoidal-visco-piezoelasticity theories", *J. Sandw. Struct. Mater.* (2017), 1099636217720373.

[Hajmohammad et al. 2018] M. H. Hajmohammad, M. B. Azizkhani, and R. Kolahchi, "Multiphase nanocomposite viscoelastic laminated conical shells subjected to magneto-hygrothermal loads: dynamic buckling analysis", *Int. J. Mech. Sci.* **137** (2018), 205–213.

[Hussein and Heyliger 1998] M. Hussein and P. Heyliger, "Three-dimensional vibrations of layered piezoelectric cylinders", *J. Eng. Mech.* (*ASCE*) **124**:11 (1998), 1294–1298.

[Jamal-Omidi and ShayanMehr 2017] M. Jamal-Omidi and M. ShayanMehr, "An experimental study on the nonlinear free vibration response of epoxy and carbon fiber-reinforced composite containing single-walled carbon nanotubes", *J. Vib. Control* **24**:19 (2017), 4529–4540.

[Kamarian et al. 2018] S. Kamarian, M. Shakeri, and M. H. Yas, "Natural frequency analysis and optimal design of CNT/fiber/polymer hybrid composites plates using mori-tanaka approach, GDQ technique, and firefly algorithm", *Polym. Compos.* **39**:5 (2018), 1433–1446.

[Ke et al. 2014] L. L. Ke, Y. S. Wang, and J. N. Reddy, "Thermo-electro-mechanical vibration of size-dependent piezoelectric cylindrical nanoshells under various boundary conditions", *Compos. Struct.* **116** (2014), 626–636.

[Keleshteri et al. 2017] M. M. Keleshteri, H. Asadi, and Q. Wang, "Postbuckling analysis of smart FG-CNTRC annular sector plates with surface-bonded piezoelectric layers using generalized differential quadrature method", *Comput. Methods Appl. Mech. Eng.* **325** (2017), 689–710.

[Kheibari and Beni 2017] F. Kheibari and Y. T. Beni, "Size dependent electro-mechanical vibration of single-walled piezoelectric nanotubes using thin shell model", *Mater. Des.* **114** (2017), 572–583.

[Khoa et al. 2019] N. D. Khoa, H. T. Thiem, and N. D. Duc, "Nonlinear buckling and postbuckling of imperfect piezoelectric S-FGM circular cylindrical shells with metal-ceramic-metal layers in thermal environment using Reddy's third-order shear deformation shell theory", *Mech. Adv. Mater. Struct.* **26**:3 (2019), 248–259.

[Lang and Xuewu 2013] Z. Lang and L. Xuewu, "Buckling and vibration analysis of functionally graded magneto-electro-thermo-elastic circular cylindrical shells", *Appl. Math. Model.* **37**:4 (2013), 2279–2292.

[Leissa 1993] A. W. Leissa, *Vibration of shells*, Acoustical Society of America, New York, 1993.

[Li et al. 2015] R. Li, P. Wang, Y. Tian, B. Wang, and G. Li, "A unified analytic solution approach to static bending and free vibration problems of rectangular thin plates", *Sci. Rep.* **5** (2015), 17054.

[Lim and Xu 2010] C. W. Lim and X. S. Xu, "Symplectic elasticity: theory and applications", *Appl. Mech. Rev.* (*ASME*) **63**:5 (2010), 050802–10.

[Mehralian and Tadi Beni 2016] F. Mehralian and Y. Tadi Beni, "Size-dependent torsional buckling analysis of functionally graded cylindrical shell", *Compos. B Eng.* **94** (2016), 11–25.

[Mehralian and Tadi Beni 2017a] F. Mehralian and Y. Tadi Beni, "Molecular dynamics analysis on axial buckling of functionalized carbon nanotubes in thermal environment", *J. Mol. Model.* **23**:12 (2017), 330.

[Mehralian and Tadi Beni 2017b] F. Mehralian and Y. Tadi Beni, "Thermo-electro-mechanical buckling analysis of cylindrical nanoshell on the basis of modified couple stress theory", *J. Mech. Sci. Technol.* **31**:4 (2017), 1773–1787.

[Mehralian and Tadi Beni 2018] F. Mehralian and Y. Tadi Beni, "Buckling of bimorph functionally graded piezoelectric cylindrical nanoshell", *Proc. Inst. Mech. Engineer. Part C: J. Mech. Eng. Sci.* **232**:19 (2018), 3538–3550.

[Mehralian et al. 2016a] F. Mehralian, Y. Tadi Beni, and R. Ansari, "On the size dependent buckling of anisotropic piezoelectric cylindrical shells under combined axial compression and lateral pressure", *Int. J. Mech. Sci.* **119** (2016), 155–169.

[Mehralian et al. 2016b] F. Mehralian, Y. Tadi Beni, and R. Ansari, "Size dependent buckling analysis of functionally graded piezoelectric cylindrical nanoshell", *Compos. Struct.* **152** (2016), 45–61.

[Mehralian et al. 2017a] F. Mehralian, Y. Tadi Beni, and M. K. Zeverdejani, "Calibration of nonlocal strain gradient shell model for buckling analysis of nanotubes using molecular dynamics simulations", *Physica B* **521** (2017), 102–111.

[Mehralian et al. 2017b] F. Mehralian, Y. Tadi Beni, and M. K. Zeverdejani, "Nonlocal strain gradient theory calibration using molecular dynamics simulation based on small scale vibration of nanotubes", *Physica B* **517** (2017), 61–69.

[Mirzavand and Eslami 2007] B. Mirzavand and M. R. Eslami, "Thermal buckling of simply supported piezoelectric FGM cylindrical shells", *J. Therm. Stresses* **30**:11 (2007), 1117–1135.

[Mirzavand and Eslami 2011] B. Mirzavand and M. R. Eslami, "A closed-form solution for thermal buckling of piezoelectric FGM hybrid cylindrical shells with temperature dependent properties", *Mech. Adv. Mater. Struct.* **18**:3 (2011), 185–193.

[Mirzavand et al. 2010] B. Mirzavand, M. R. Eslami, and M. Shakeri, "Dynamic thermal postbuckling analysis of piezoelectric functionally graded cylindrical shells", *J. Therm. Stresses* **33**:7 (2010), 646–660.

[Mirzavand et al. 2013] B. Mirzavand, M. R. Eslami, and J. N. Reddy, "Dynamic thermal postbuckling analysis of shear deformable piezoelectric-FGM cylindrical shells", *J. Therm. Stresses* **36**:3 (2013), 189–206.

[Mirzavand et al. 2016] B. Mirzavand, P. Rezapour, and M. Bohlooly, "Thermal buckling of shallow/nonshallow piezoelectric-composite cylindrical shells", *Mech. Adv. Mater. Struct.* **23**:10 (2016), 1236–1243.

[Mohammadimehr et al. 2014] M. Mohammadimehr, M. Moradi, and A. Loghman, "Influence of the elastic foundation on the free vibration and buckling of thin-walled piezoelectric-based FGM cylindrical shells under combined loadings", *J. Solid Mech.* **6**:4 (2014), 347–365.

[Mohammadimehr et al. 2016] M. Mohammadimehr, B. Rousta Navi, and A. Ghorbanpour Arani, "Modified strain gradient Reddy rectangular plate model for biaxial buckling and bending analysis of double-coupled piezoelectric polymeric nanocomposite reinforced by FG-SWNT", *Compos. B Eng.* **87** (2016), 132–148.

[Mosallaie Barzoki et al. 2012] A. A. Mosallaie Barzoki, A. Ghorbanpour Arani, R. Kolahchi, and M. R. Mozdianfard, "Electro-thermo-mechanical torsional buckling of a piezoelectric polymeric cylindrical shell reinforced by DWBNNTs with an elastic core", *Appl. Math. Model.* **36**:7 (2012), 2983–2995.

[Mosallaie Barzoki et al. 2013] A. A. Mosallaie Barzoki, A. Ghorbanpour Arani, R. Kolahchi, M. R. Mozdianfard, and A. Loghman, "Nonlinear buckling response of embedded piezoelectric cylindrical shell reinforced with BNNT under electro–thermo-mechanical loadings using HDQM", *Compos. B Eng.* **44**:1 (2013), 722–727.

[Ni et al. 2017] Y. Ni, Z. Tong, D. Rong, Z. Zhou, and X. Xu, "A new Hamiltonian-based approach for free vibration of a functionally graded orthotropic circular cylindrical shell embedded in an elastic medium", *Thin-Walled Struct.* **120** (2017), 236–248.

[Ni et al. 2018] Y. Ni, Z. Tong, D. Rong, Z. Zhou, and X. Xu, "Accurate thermal buckling analysis of functionally graded orthotropic cylindrical shells under the symplectic framework", *Thin-Walled Struct.* **129** (2018), 1–9.

[Ninh 2018] D. G. Ninh, "Nonlinear thermal torsional post-buckling of carbon nanotube-reinforced composite cylindrical shell with piezoelectric actuator layers surrounded by elastic medium", *Thin-Walled Struct.* **123** (2018), 528–538.

[Pietrzakowski 2008] M. Pietrzakowski, "Piezoelectric control of composite plate vibration: effect of electric potential distribution", *Comput. Struct.* **86**:9 (2008), 948–954.

[Rafiee et al. 2013] M. Rafiee, J. Yang, and S. Kitipornchai, "Thermal bifurcation buckling of piezoelectric carbon nanotube reinforced composite beams", *Comput. Math. Appl.* **66**:7 (2013), 1147–1160.

[Rafiee et al. 2014] M. Rafiee, X. Q. He, and K. M. Liew, "Non-linear dynamic stability of piezoelectric functionally graded carbon nanotube-reinforced composite plates with initial geometric imperfection", *Int. J. Non-Linear Mech.* **59** (2014), 37–51.

[Rafiee et al. 2019] M. Rafiee, F. Nitzsche, and M. R. Labrosse, "Fabrication and experimental evaluation of vibration and damping in multiscale graphene/fiberglass/epoxy composites", *J. Compos. Mater.* **53**:15 (2019), 2105–2118.

[Rotter 2014] J. M. Rotter, "Cylindrical shells under axial compression", pp. 66–111 in *Buckling of thin metal shells*, edited by J. G. Teng and J. M. Rotter, CRC Press, 2014.

[SafarPour et al. 2019] H. SafarPour, B. Ghanbari, and M. Ghadiri, "Buckling and free vibration analysis of high speed rotating carbon nanotube reinforced cylindrical piezoelectric shell", *Appl. Math. Model.* **65** (2019), 428–442.

[Sahmani et al. 2016] S. Sahmani, M. M. Aghdam, and A. H. Akbarzadeh, "Size-dependent buckling and postbuckling behavior of piezoelectric cylindrical nanoshells subjected to compression and electrical load", *Mater. Des.* **105** (2016), 341–351.

[Salehi-Khojin and Jalili 2008] A. Salehi-Khojin and N. Jalili, "Buckling of boron nitride nanotube reinforced piezoelectric polymeric composites subject to combined electro-thermo-mechanical loadings", *Compos. Sci. Technol.* **68**:6 (2008), 1489–1501.

[Saviz et al. 2007] M. R. Saviz, M. Shakeri, and M. H. Yas, "Electroelastic fields in a layered piezoelectric cylindrical shell under dynamic load", *Smart Mater. Struct.* **16**:5 (2007), 1683–1695.

[Shen 2001] H.-S. Shen, "Postbuckling analysis of axially-loaded laminated cylindrical shells with piezoelectric actuators", *Eur. J. Mech. A Solids* **20**:6 (2001), 1007–1022.

[Shen 2002a] H.-S. Shen, "Postbuckling of laminated cylindrical shells with piezoelectric actuators under combined external pressure and heating", *Int. J. Solids Struct.* **39**:16 (2002), 4271–4289.

[Shen 2002b] H.-S. Shen, "Thermal postbuckling analysis of laminated cylindrical shells with piezoelectric actuators", *Compos. Struct.* **55**:1 (2002), 13–22.

[Shen 2005] H.-S. Shen, "Postbuckling of axially loaded FGM hybrid cylindrical shells in thermal environments", *Compos. Sci. Technol.* **65**:11-12 (2005), 1675–1690.

[Shen 2009] H.-S. Shen, "A comparison of post-buckling behavior for FGM cylindrical shells with piezoelectric fiber reinforced composite actuators", *J. Eng. Mater. Technol.* (*ASME*) **131**:3 (2009), 031010–031010–11.

[Shen 2010] H.-S. Shen, "Buckling and postbuckling of anisotropic laminated cylindrical shells with piezoelectric fiber reinforced composite actuators", *Mech. Adv. Mater. Struct.* **17**:4 (2010), 268–279.

[Shen and Li 2002] H.-S. Shen and Q. S. Li, "Postbuckling of cross-ply laminated cylindrical shells with piezoelectric actuators under complex loading conditions", *Int. J. Mech. Sci.* **44**:8 (2002), 1731–1754.

[Shen and Noda 2007] H.-S. Shen and N. Noda, "Postbuckling of pressure-loaded FGM hybrid cylindrical shells in thermal environments", *Compos. Struct.* **77**:4 (2007), 546–560.

[Shen and Xiang 2007] H.-S. Shen and Y. Xiang, "Postbuckling of pressure-loaded piezolaminated cylindrical shells with temperature dependent properties", *Int. J. Struct. Stab. Dyn.* **7**:1 (2007), 1–22.

[Sheng and Wang 2010] G. G. Sheng and X. Wang, "Thermoelastic vibration and buckling analysis of functionally graded piezoelectric cylindrical shells", *Appl. Math. Model.* **34**:9 (2010), 2630–2643.

[Sun et al. 2013] J. Sun, X. Xu, and C. W. Lim, "Accurate symplectic space solutions for thermal buckling of functionally graded cylindrical shells", *Compos. B Eng.* **55** (2013), 208–214.

[Sun et al. 2014a] J. Sun, X. Xu, and C. W. Lim, "Buckling of functionally graded cylindrical shells under combined thermal and compressive loads", *J. Therm. Stresses* **37**:3 (2014), 340–362.

[Sun et al. 2014b] J. Sun, X. Xu, and C. W. Lim, "Torsional buckling of functionally graded cylindrical shells with temperature-dependent properties", *Int. J. Struct. Stab. Dyn.* **14**:01 (2014), 1350048.

[Sun et al. 2016] J. Sun, X. Xu, C. W. Lim, Z. Zhou, and S. Xiao, "Accurate thermo-electro-mechanical buckling of shear deformable piezoelectric fiber-reinforced composite cylindrical shells", *Compos. Struct.* **141** (2016), 221–231.

[Sun et al. 2018] J. Sun, Z. Wang, Z. Zhou, X. Xu, and C. W. Lim, "Surface effects on the buckling behaviors of piezoelectric cylindrical nanoshells using nonlocal continuum model", *Appl. Math. Model.* **59** (2018), 341–356.

[Tadi Beni and Mehralian 2016] Y. Tadi Beni and F. Mehralian, "The effect of small scale on the free vibration of functionally graded truncated conical shells", *J. Mech. Mater. Struct.* **11**:2 (2016), 91–112.

[Tadi Beni et al. 2015] Y. Tadi Beni, F. Mehralian, and H. Razavi, "Free vibration analysis of size-dependent shear deformable functionally graded cylindrical shell on the basis of modified couple stress theory", *Compos. Struct.* **120** (2015), 65–78.

[Tadi Beni et al. 2016] Y. Tadi Beni, F. Mehralian, and H. Zeighampour, "The modified couple stress functionally graded cylindrical thin shell formulation", *Mech. Adv. Mater. Struct.* **23**:7 (2016), 791–801.

[Tan and Tong 2001a] P. Tan and L. Tong, "Micro-electromechanics models for piezoelectric-fiber-reinforced composite materials", *Compos. Sci. Technol.* **61**:5 (2001), 759–769.

[Tan and Tong 2001b] P. Tan and L. Tong, "Micromechanics models for non-linear behavior of piezo-electric fiber reinforced composite materials", *Int. J. Solids Struct.* **38**:50-51 (2001), 8999–9032.

[Teng 1996] J. G. Teng, "Buckling of thin shells: recent advances and trends", *Appl. Mech. Rev. (ASME)* **49**:4 (1996), 263–274.

[Teng and Rotter 2014] J. G. Teng and J. M. Rotter, "Buckling of thin shells: an overview", pp. 25–65 in *Buckling of thin metal shells*, CRC Press, 2014.

[Ueberschlag 2001] P. Ueberschlag, "PVDF piezoelectric polymer", *Sens. Rev.* **21**:2 (2001), 118–126.

[Wang 2002] Q. Wang, "On buckling of column structures with a pair of piezoelectric layers", *Eng. Struct.* **24**:2 (2002), 199–205.

[Wang and Qin 2007] J.-S. Wang and Q.-H. Qin, "Symplectic model for piezoelectric wedges and its application in analysis of electroelastic singularities", *Philos. Mag.* **87**:2 (2007), 225–251.

[Wu and Chang 2014] C.-P. Wu and S.-K. Chang, "Stability of carbon nanotube-reinforced composite plates with surface-bonded piezoelectric layers and under bi-axial compression", *Compos. Struct.* **111** (2014), 587–601.

[Wu et al. 2016] H. Wu, S. Kitipornchai, and J. Yang, "Thermo-electro-mechanical postbuckling of piezoelectric FG-CNTRC beams with geometric imperfections", *Smart Mater. Struct.* **25**:9 (2016), 095022.

[Yamaki 1984] N. Yamaki, *Elastic stability of circular cylindrical shells*, North-Holland, Amsterdam, 1984.

[Yang et al. 2015] J. Yang, L.-L. Ke, and C. Feng, "Dynamic buckling of thermo-electro-mechanically loaded FG-CNTRC beams", *Int. J. Struct. Stab. Dyn.* **15**:8 (2015), 1540017.

[Yao et al. 2009] W. Yao, W. Zhong, and C. W. Lim, *Symplectic elasticity*, World Scientific, 2009.

[Zeighampour and Tadi Beni 2014] H. Zeighampour and Y. Tadi Beni, "Cylindrical thin-shell model based on modified strain gradient theory", *Int. J. Eng. Sci.* **78** (2014), 27–47.

[Zhu et al. 2017] C.-S. Zhu, X.-Q. Fang, and J.-X. Liu, "Surface energy effect on buckling behavior of the functionally graded nano-shell covered with piezoelectric nano-layers under torque", *Int. J. Mech. Sci.* **133** (2017), 662–673.

SHENGBO ZHU: zhushengbo@mail.dlut.edu.cn
State Key Laboratory of Structural Analysis for Industrial Equipment and Department of Engineering Mechanics,
Dalian University of Technology, Dalian, 116023, China

YIWEN NI: nyw2009213@mail.dlut.edu.cn
State Key Laboratory of Structural Analysis for Industrial Equipment and Department of Engineering Mechanics,
Dalian University of Technology, Dalian, 116024, China

JIABIN SUN: jbsun1983@dlut.edu.cn
State Key Laboratory of Structural Analysis for Industrial Equipment and School of Ocean Science and Technology,
Dalian University of Technology, Panjin, 124221, China

ZHENZHEN TONG: tongzhzh@163.com
College of Locomotive and Rolling Stock Engineering, Dalian Jiaotong University, Dalian, 116028, China

ZHENHUAN ZHOU: zhouzh@dlut.edu.cn
State Key Laboratory of Structure Analysis for Industrial Equipment and Department of Engineering Mechanics,
Dalian University of Technology, Dalian, 116024, China

XINSHENG XU: xsxu@dlut.edu.cn
Department of Engineering Mechanics, Dalian University of Technology, State Key Laboratory for Structural Analysis for
Industrial Equipment, Dalian, 116024, China

JOURNAL OF MECHANICS OF MATERIALS AND STRUCTURES

msp.org/jomms

Founded by Charles R. Steele and Marie-Louise Steele

Journal of Mechanics of Materials and Structures